Relic density of neutralino dark matter in the MSSM with *CP* violation

G. Bélanger,[1] F. Boudjema,[1] S. Kraml,[2] A. Pukhov,[3] and A. Semenov[4]
[1]*LAPTH, 9 Chemin de Bellevue, B.P. 110, F-74941 Annecy-le-Vieux, France*
[2]*CERN, Department of Physics, Theory Division, CH-1211 Geneva 23, Switzerland*
[3]*Skobeltsyn Institute of Nuclear Physics, Moscow State University, Moscow 119992, Russia*
[4]*Joint Institute for Nuclear Research (JINR), 141980, Dubna, Russia*
(Received 28 April 2006; published 16 June 2006)

We calculate the relic density of dark matter in the MSSM with *CP* violation. We analyze various scenarios of neutralino annihilation: the cases of a *b*-ino, *b*-ino–*W*-ino and *b*-ino–Higgsino LSP, annihilation through Higgs, as well as sfermion coannihilation scenarios. Large phase effects are found—on the one hand, due to shifts in the masses; on the other hand, due to modifications of the couplings. Taking special care to disentangle the effects in masses and couplings, we demonstrate that the presence of *CP* phases can have a significant influence on the neutralino relic abundance. Typical variations in Ωh^2 solely from modifications in the couplings are $\mathcal{O}$ (10%–100%), but can reach an order of magnitude in some cases.

DOI: 10.1103/PhysRevD.73.115007 PACS numbers: 12.60.Jv, 95.35.+d

I. INTRODUCTION

With the conclusive evidence for a significant component of cold dark matter (CDM) in the Universe, there is considerable interest, both at the theoretical and experimental level, to identify this CDM and analyze its properties; see [1] for a recent review. In particular, if the CDM consists of a new weakly interacting massive particle (WIMP), as predicted in generic new physics models with a discrete symmetry that ensures the stability of the lightest particle, the next generation of colliders has good prospects to discover it. Being electrically neutral and stable, the WIMP escapes the detector as missing energy and momentum. The preferred discovery channels therefore rely on the production of other new particles present in the theory and their decays into the CDM candidate. By measuring the properties and decay kinematics of these new particles, one should then be able to determine the properties of the WIMP. If the measurements are precise enough, this allows one to predict the annihilation cross sections and hence the thermal relic density of the CDM candidate, thus checking the consistency between a particular model of new physics and cosmology.

Indeed, particle physics models trying to explain the dark matter are constrained by recent precision cosmological measurements. These are most notably the data from WMAP [2,3] and SDSS [4], which imply a (dominantly) cold dark matter density of

$$0.0945 < \Omega_{\rm CDM} h^2 < 0.1287 \qquad (1)$$

at 2σ. In the following we will refer to Eq. (1) as the WMAP range.

The relic density of dark matter has been discussed extensively in the framework of the most popular model for new physics, low-scale supersymmetry (SUSY) with *R*-parity conservation. Especially if the lightest supersymmetric particle (LSP) is the lightest neutralino, this provides a good cold dark matter candidate [5,6]. For the standard picture of thermal freeze-out [7], assuming no additional nonthermal production mechanism, comprehensive public codes that compute the relic density of the neutralino LSP are available today: MICROMEGAS [8,9], DARKSUSY [10], and ISARED [11]. Many analyses of neutralino dark matter were performed in the minimal supersymmetric standard model (MSSM), whose parameters are defined at the weak scale (see e.g. [12–14]) in the constrained MSSM (CMSSM) and minimal supergravity (mSUGRA) models [15–25], and in other models with the parameters defined at the unification scale [26–34].

These studies showed that in the MSSM there are only a few mechanisms that provide the correct amount of neutralino annihilation, consistent with the WMAP range Eq. (1): annihilation of a *b*-ino LSP into fermion pairs through *t*-channel sfermion exchange in the case of very light sparticles; annihilation of a mixed *b*-ino–Higgsino or *b*-ino–*W*-ino LSP into gauge boson pairs through *t*-channel chargino and neutralino exchange, and into top-quark pairs through *s*-channel *Z* exchange; and finally annihilation near a Higgs resonance (the so-called Higgs funnel). Furthermore, coannihilation processes with sparticles that are close in mass with the LSP may bring Ωh^2 in the desired range. In particular, coannihilation with light sfermions can help to reduce the relic density of a *b*-ino-like LSP. Here note that coannihilation generically occurs when there is a small mass gap between the LSP and the next-to-lightest SUSY particle (NLSP). In scenarios with a Higgsino or *W*-ino LSP, one has in fact a mass-degenerate triplet of Higgsinos or *W*-inos, and coannihilations are so efficient that Ωh^2 turns out much too small, unless the LSP has a mass of order TeV. In the case that Ωh^2 is too low one would need, for instance, a significant contribution from nonthermal production.

Most of these previous analyses assumed that *CP* is conserved, although *CP*-violating phases are generic in

the MSSM. Here note that, given the Higgs mass bound $m_h > 114$ GeV from CERN LEP [35], the Cabibbo-Kobayashi-Maskawa description of *CP* violation (CPV) in the SM is not sufficient to generate the correct baryon asymmetry in the Universe. One possible solution to this problem is leptogenesis. Another solution is electroweak baryogenesis through new sources of *CP* violation beyond the SM. Electroweak baryogenesis in the MSSM with *CP* violation (CPV-MSSM) has been studied in [36–38]; see also references therein. For a strongly first-order phase transition, it relies on the existence of a light stop [39–42].

The parameters that can have *CP* phases are the gaugino and Higgsino mass parameters and the trilinear sfermion-Higgs couplings. Although constrained by electric dipole moments, nonzero phases can significantly influence the phenomenology of SUSY particles. They can also have a strong impact on the Higgs sector, inducing scalar-pseudoscalar mixing through loop effects [43–45]. This can, in turn, have a potentially dramatic effect on the relic density prediction in the Higgs-funnel region: neutralino annihilation through s-channel scalar exchange is p-wave suppressed; at small velocities it is dominated by pseudoscalar exchange. In the presence of phases, both heavy Higgs bosons can, for instance, acquire a pseudoscalar component and hence significantly contribute to neutralino annihilation even at small velocities. Likewise, when only one of the resonances is accessible to the neutralino annihilation, large effects can be expected by changing the scalar/pseudoscalar content of this resonance. Last but not least, the couplings of the LSP to other sparticles depend on the phases, and so will all the annihilation and coannihilation cross sections, even though this is not a *CP*-violating (*CP*-odd) effect.

Consequences of complex parameters for the relic density of neutralinos have so far been considered in the literature only for specific cases. The effect of a phase in the squark left-right mixing was shown to enhance the cross section for neutralino annihilation into fermion pairs [46], but the important sfermion coannihilation effects were not included. In [47], the influence of phases was discussed for various cases of gaugino-Higgsino mixing, taking into account CPV in the Higgs sector. However, coannihilations were again disregarded. Reference [48] discussed phase effects in neutralino annihilation through Higgs exchange in the CMSSM at large $\tan\beta$. Likewise, Ref. [49] examined a very specific case, namely, the dependence of Ωh^2 on phases that arise through supersymmetric loop corrections to the b-quark mass in SUGRA models with Yukawa unification. For the general MSSM, the effects of a phase in the trilinear coupling of the top squark on the neutralino annihilation near a Higgs resonance were discussed in [50] and more recently in [51], but without analyzing the phase dependence of Ωh^2. Finally, the case of coannihilation with very light stops was discussed in [36,38] in the framework of electroweak baryogenesis. Also, these latter papers considered only a few fixed values of ϕ_μ and did not study the phase dependence of Ωh^2 in detail. It is, moreover, important to note that all the above-mentioned publications studied the impact of phases solely in terms of SUSY-breaking parameters, without discussing that part of the phase effects are due to changes in the masses of the involved particles.

A complete and coherent analysis of the relic density of neutralinos in the CPV-MSSM is therefore still missing, and this is the gap we intend to fill with this paper. We perform a comprehensive analysis of the impact of *CP* phases on the relic density of neutralino dark matter, consistently taking into account phases in *all* annihilation and coannihilation channels. To this end, we realized the implementation of the CPV-MSSM within MICROMEGAS 2.0 [52,53]. For the computation of masses, mixings and effective couplings in the Higgs sector, we rely on CPSUPERH [54]. We further take into account collider constraints from sparticle and Higgs searches, as well as the constraint arising from the electric dipole moment of the electron [55].

Besides realizing the complete calculation of the relic density of neutralinos in the CPV-MSSM, we analyze in detail the above-mentioned scenarios of neutralino annihilation and coannihilation, for which the LSP is a ''good'' CDM candidate. We find indeed a large impact from phases due to modifications in the sparticle couplings (through changes in the mixing matrices) but also due to changes in the physical masses. Some of the largest effects are, in fact, due to kinematics. This should be expected as the relic density is often very sensitive to masses, in particular, to the exact mass difference between the LSP and NLSP in coannihilation processes, or, in the case of annihilation near an s-channel Higgs resonance, to the difference between twice the LSP mass and the mass of the Higgs. In these scenarios, setting apart the purely kinematic effects hence somewhat tames the huge effects due to *CP* phases found in some of the previous studies listed above. On the other hand, we also find cases where the phase dependences of masses and couplings work against each other, and taking out the kinematic effects actually enhances the phase dependence of the number density. There are even cases in which, for fixed MSSM parameters, Ωh^2 decreases with increasing phase, but once the masses are kept fixed, Ωh^2 actually grows. Since what are relevant to experiments are the physical observables (masses, branching ratios, etc.) rather than the underlying parameters, we take special care in our analysis to disentangle effects arising from changes in the couplings from purely kinematic effects.

After a description of the model in Sec. II and its implementation into MICROMEGAS 2.0 in Sec. III, we present in Sec. IV our results for the typical scenarios of neutralino annihilation: the mixed b-ino–Higgsino case with annihilation into W pairs, rapid annihilation near a Higgs reso-

nance, the b-ino-like LSP with light sfermions (t-channel and coannihilation regions), and finally the mixed b-ino–W-ino scenario with neutralino-chargino coannihilation. In Sec. V, we give a summary and conclusions. For completeness, the Lagrangian for sparticle interactions in the CPV-MSSM is given in the Appendix.

II. THE MSSM WITH *CP* PHASES

We consider the general MSSM with parameters defined at the weak scale. In this framework, the gaugino and Higgsino mass parameters and the trilinear couplings can have complex phases, $M_i = |M_i|e^{i\phi_i}$, $\mu = |\mu|e^{i\phi_\mu}$ and $A_f = |A_f|e^{i\phi_f}$. Not all of these phases, however, are relevant to our analysis. In particular, the phase of M_2 can always be rotated away, while the phase of M_3 is mostly relevant for the colored sector, so we neglect it in this study. Among the trilinear couplings, A_t has the largest effect on the Higgs sector, and can thus potentially play an important role for the relic density. The phase of the selectron coupling A_e, as the phase of all light sfermions, is irrelevant for the relic density; it has to, however, be taken into account since it contributes to electric dipole moments (EDMs).

In the following, we explain our notation and conventions. We hereby basically follow the notation in CPSUPERH and use the SUSY Les Houches Accord (SLHA) [56]. We also discuss some of the most relevant couplings. For the complete interaction Lagrangian, see the Appendix and Ref. [54].

Neutralinos.—The neutralino mass matrix in the b-ino–W-ino–Higgsino basis $\psi_j^0 = (-i\lambda', -i\lambda^3, \psi_{H_1}^0, \psi_{H_2}^0)$ is

$$\mathcal{M}_N = \begin{pmatrix} M_1 & 0 & -m_Z s_W c_\beta & m_Z s_W s_\beta \\ 0 & M_2 & m_Z c_W c_\beta & -m_Z c_W s_\beta \\ -m_Z s_W c_\beta & m_Z c_W c_\beta & 0 & -\mu \\ m_Z s_W s_\beta & -m_Z c_W s_\beta & -\mu & 0 \end{pmatrix} \tag{2}$$

with $s_W = \sin\theta_W$, $c_W = \cos\theta_W$, $s_\beta = \sin\beta$, $c_\beta = \cos\beta$ and $\tan\beta = v_2/v_1$ ($v_{1,2}$ being the vacuum expectation values of the two Higgs fields $H_{1,2}$). This matrix is diagonalized by a unitary mixing matrix N,

$$N^* \mathcal{M}_N N^\dagger = \mathrm{diag}(m_{\tilde{\chi}_1^0}, m_{\tilde{\chi}_2^0}, m_{\tilde{\chi}_3^0}, m_{\tilde{\chi}_4^0}), \tag{3}$$

where $m_{\tilde{\chi}_i^0}$, $i = 1, \ldots, 4$, are the (non-negative) masses of the physical neutralino states with $m_{\tilde{\chi}_1^0} < \ldots < m_{\tilde{\chi}_4^0}$. The lightest neutralino is then decomposed as

$$\tilde{\chi}_1^0 = N_{11}\tilde{B} + N_{12}\tilde{W} + N_{13}\tilde{H}_1 + N_{14}\tilde{H}_2 \tag{4}$$

with the b-ino (f_B), W-ino (f_W) and Higgsino (f_H) fractions defined as

$$f_B = |N_{11}|^2, \qquad f_W = |N_{12}|^2, \qquad f_H = |N_{13}|^2 + |N_{14}|^2. \tag{5}$$

The LSP will hence be mostly b-ino, W-ino, or Higgsino according to the smallest mass parameter in Eq. (2), M_1, M_2, or μ, respectively.

Charginos.—The chargino mass matrix in SLHA notation,[1]

$$\mathcal{M}_C = \begin{pmatrix} M_2 & \sqrt{2} m_W \sin\beta \\ \sqrt{2} m_W \cos\beta & \mu \end{pmatrix}, \tag{6}$$

is diagonalized by two unitary matrices U and V,

$$U^* \mathcal{M}_C V^\dagger = \mathrm{diag}(m_{\tilde{\chi}_1^\pm}, m_{\tilde{\chi}_2^\pm}), \tag{7}$$

with the eigenvalues again being mass ordered. The chargino sector will be relevant mainly because t-channel chargino exchange dominates the $\tilde{\chi}_1^0\tilde{\chi}_1^0 \to W^+W^-$ cross section, which is often the main annihilation process when the LSP has a sizable Higgsino component. The relevant Lagrangian is

$$\mathcal{L}_{\tilde{\chi}_j^0\tilde{\chi}_i^+W^-} = g W_\mu^- \bar{\tilde{\chi}}_j^0 \gamma^\mu (O_{ji}^L P_L + O_{ji}^R P_R)\tilde{\chi}_i^+ + \mathrm{H.c.} \tag{8}$$

with

$$O_{ji}^L = N_{j2}V_{i1}^* - \frac{1}{\sqrt{2}} N_{j4} V_{i2}^*, \qquad O_{ji}^R = N_{j2}^* U_{i1} + \frac{1}{\sqrt{2}} N_{j3}^* U_{i2}. \tag{9}$$

These expressions are the same as for the real MSSM and show that the $\tilde{\chi}_1^0\tilde{\chi}_i^\pm W^\mp$ coupling vanishes in the case of a pure b-ino LSP. Note that this coupling also enters the chargino coannihilation processes into gauge boson pairs which are important in some specific scenarios. Nonzero phases will affect directly the masses of the charginos and neutralinos as well as the couplings through shifts in the mixing matrices.

Sfermions.—Ignoring intergenerational mixing, the sfermion mass matrices are

$$\mathcal{M}_{\tilde{f}}^2 = \begin{pmatrix} m_{\tilde{f}_L}^2 & h_f^* a_f^* \\ h_f a_f & m_{\tilde{f}_R}^2 \end{pmatrix} \tag{10}$$

with

$$m_{\tilde{f}_L}^2 = M_{\{\tilde{Q},\tilde{L}\}}^2 + m_Z^2 \cos 2\beta (I_{3L}^f - e_f \sin^2\theta_W) + m_f^2, \tag{11}$$

$$m_{\tilde{f}_R}^2 = M_{\{\tilde{U},\tilde{D},\tilde{R}\}}^2 + e_f m_Z^2 \cos 2\beta \sin^2\theta_W + m_f^2, \tag{12}$$

[1]Here note that in CPSUPERH, $\mathcal{M}_C \to \mathcal{M}_C^T$.

and

$$a_t = (A_t v_2 - \mu^* v_1)/\sqrt{2}, \tag{13}$$

$$a_{b,\tau} = (A_{b,\tau} v_1 - \mu^* v_2)/\sqrt{2}, \tag{14}$$

for $\tilde{f} = \tilde{t}, \tilde{b}, \tilde{\tau}$. Here $M_{\{\tilde{Q},\tilde{L}\}}$, $M_{\{\tilde{U},\tilde{D},\tilde{R}\}}$ are the left and right sfermion mass parameters; m_f, e_f, and I_3^f are the mass, electric charge, and the third component of the weak isospin of the partner fermion, respectively, and h_f denote the Yukawa couplings, $h_t = \sqrt{2} m_t/v \cos\beta$ and $h_{b,\tau} = \sqrt{2} m_{b,\tau}/v \sin\beta$ at tree level. Here, $v^2 = v_1^2 + v_2^2$. The mass matrix $\mathcal{M}^2_{\tilde{f}}$ is diagonalized by a unitary matrix $R^{\tilde{f}}$ such that

$$R^{\tilde{f}\dagger} \mathcal{M}^2_{\tilde{f}} R^{\tilde{f}} = \mathrm{diag}(m^2_{\tilde{f}_1}, m^2_{\tilde{f}_2}) \tag{15}$$

with $m_{\tilde{f}_1} \leq m_{\tilde{f}_2}$ and $(\tilde{f}_L, \tilde{f}_R)^T = R^{\tilde{f}}(\tilde{f}_1, \tilde{f}_2)^T$. The relevant sfermion interactions are given in the Appendix.

Neutral Higgs bosons.—In the *CP*-conserving MSSM, the Higgs sector consists of two *CP*-even states h^0, H^0 and one *CP*-odd state A^0. Allowing for *CP*-violating phases induces a mixing between these three states through loop corrections. The resulting mass eigenstates h_1, h_2, h_3 (with $m_{h_1} < m_{h_2} < m_{h_3}$ by convention) are no longer eigenstates of *CP*. The Higgs mixing matrix is defined by[2]

$$(\phi_1, \phi_2, a)^T_a = H_{ai}(h_1, h_2, h_3)^T_i. \tag{16}$$

Because of the mixing between the neutral scalar and pseudoscalar states, it is preferable to use the charged Higgs mass, m_{H^+}, as an independent parameter. In what follows we will mainly be concerned with the couplings of the lightest neutralino to Higgs bosons that govern the neutralino annihilation cross section via Higgs exchange. The Lagrangian for such interactions is

$$\mathcal{L}_{\tilde{\chi}^0_1 \tilde{\chi}^0_1 h_i} = -\frac{g}{2} \sum_{i=1}^{3} \bar{\tilde{\chi}}^0_1 (g^S_{h_i \tilde{\chi}^0_1 \tilde{\chi}^0_1} + i\gamma_5 g^P_{h_i \tilde{\chi}^0_1 \tilde{\chi}^0_1}) \tilde{\chi}^0_1 h_i \tag{17}$$

with the scalar and pseudoscalar couplings corresponding to the real and imaginary parts of the same expression:

$$g^S_{h_i \tilde{\chi}^0_1 \tilde{\chi}^0_1} = \mathrm{Re}[(N^*_{12} - t_W N^*_{11})(H_{1i} N^*_{13} - H_{2i} N^*_{14} - i H_{3i}(s_\beta N^*_{13} - c_\beta N^*_{14}))], \tag{18}$$

$$g^P_{h_i \tilde{\chi}^0_1 \tilde{\chi}^0_1} = -\mathrm{Im}[(N^*_{12} - t_W N^*_{11})(H_{1i} N^*_{13} - H_{2i} N^*_{14} - i H_{3i}(s_\beta N^*_{13} - c_\beta N^*_{14}))]. \tag{19}$$

For real parameters, one recovers the (h^0, H^0, A^0) couplings by taking for the pseudoscalar, A^0, $H_{33} = 1$ and all other $H_{ij} = 0$, while for the scalar Higgs couplings, the only nonzero elements are $H_{11} = -H_{22} = -\sin\alpha$ and $H_{21} = H_{12} = \cos\alpha$. The LSP couplings to neutral Higgs bosons will clearly be affected both by phases in the neutralino sector which modify the neutralino mixing, as well as by phases which induce scalar-pseudoscalar mixing in the Higgs sector. Indeed, in the MSSM the Higgs *CP* mixing is induced by loops involving top squarks and is proportional to $\mathrm{Im}(A_t \mu)/(m^2_{\tilde{t}_2} - m^2_{\tilde{t}_1})$ [57]. Thus a large mixing is expected when $\mathrm{Im}(A_t \mu)$ is comparable to the stop masses squared. Note that the masses of the physical Higgs bosons also depend on the phases of A_t and μ. In particular, a large mass splitting between the heavy states is found for large values of μA_t. For a more detailed discussion of Higgs masses and couplings in the CPV-MSSM, we refer to [54].

[2]In CPSUPERH, the Higgs mixing matrix is denoted O_{ai}.

III. RELIC DENSITY COMPUTATION AND IMPLEMENTATION OF THE CPV-MSSM INTO MICROMEGAS

The computation of the relic density of dark matter is by now standard [58,59]. It relies on solving the evolution equation for the abundance, defined as the number density divided by the entropy density,

$$\frac{dY}{dT} = \sqrt{\frac{\pi g_*(T)}{45}} M_p \langle \sigma v \rangle (Y(T)^2 - Y_{\mathrm{eq}}(T)^2) = A(T)(Y(T)^2 - Y_{\mathrm{eq}}(T)^2), \tag{20}$$

where g_* is an effective number of degrees of freedom [58], M_p is the Planck mass and $Y_{\mathrm{eq}}(T)$ the thermal equilibrium abundance, and is $\langle \sigma v \rangle$ the relativistic thermally averaged annihilation cross section of superparticles summed over all channels. It is given by

$$\langle \sigma v \rangle = \frac{\sum_{i,j} g_i g_j \int_{(m_i+m_j)^2} ds \sqrt{s} K_1(\sqrt{s}/T) p^2_{ij} \sum_{k,l} \sigma_{ij;kl}(s)}{2T(\sum_i g_i m_i^2 K_2(m_i/T))^2}, \tag{21}$$

with g_i the number of degrees of freedom, $\sigma_{ij;kl}$ the total cross section for annihilation of a pair of supersymmetric particles with masses m_i, m_j into some standard model particles (k, l), and $p_{ij}(\sqrt{s})$ the momentum (total energy) of the incoming particles in their center-of-mass frame. Integrating Eq. (20) from $T = \infty$ to $T = T_0$ gives the present-day abundance $Y(T_0)$ needed in the evaluation of the relic density,

$$\Omega_{\mathrm{LSP}} h^2 = \frac{s(T_0) h^2}{\rho_{cr}} M_{\mathrm{LSP}} Y(T_0) = 2.742 \times 10^8 \frac{M_{\mathrm{LSP}}}{\mathrm{GeV}} Y(T_0) \tag{22}$$

where $s(T_0)$ is the entropy density at the present time and h the normalized Hubble constant. The present-day energy density is then simply expressed as $\rho_{\mathrm{LSP}} = 10.54 \Omega h^2$ (GeV/m^3).

To compute the relic density, MICROMEGAS solves the equation for the abundance, Eq. (20), numerically without any approximation. In addition, MICROMEGAS also estimates the relative contribution of each individual annihilation or coannihilation channel to the relic density. For this specific purpose, the freeze-out approximation is used: below the freeze-out temperature T_f, $Y_{\rm eq} \ll Y$, and Eq. (20) can be integrated,

$$\frac{1}{Y(T_0)} = \frac{1}{Y(T_f)} + \int_{T_0}^{T_f} A(T)dT. \tag{23}$$

It turns out that $M_{\rm LSP}/T_f \approx 25$ (for more details see [8,58]). In this case, the first term in Eq. (23) is suppressed, and one can approximate $1/\Omega$ by a sum over the different annihilation channels:

$$\frac{1}{\Omega h^2} \approx \sum_{i,j,k,l} \frac{1}{\omega_{ij;kl} h^2} \tag{24}$$

where

$$\omega_{ij;kl} = \frac{s(T_0) M_{\rm LSP}}{\rho_{\rm cr}} \int_{T_0}^{T_f} \sqrt{\frac{\pi g_*(T)}{45}} M_p \times \frac{g_i g_j \int ds \sqrt{s} K_1(\sqrt{s}/T) p_{ij}^2 \sigma_{ij;kl}(s)}{2T(\sum_{i'} g_{i'} m_{i'}^2 K_2(m_{i'}/T))^2} dT. \tag{25}$$

Note that this method gives, to a good approximation, the contribution of individual channels, although the value of Ωh^2 is slightly overestimated as compared to the exact value obtained by solving directly the evolution equation for the abundance as described above.

To perform this computation for the CPV-MSSM, we are using MICROMEGAS 2.0 [52], an extension of MICROMEGAS 1.3 [8,9] that allows the computation of the relic density of dark matter within generic particle physics models that feature a stable weakly interacting particle. Within this framework we have implemented the CPV-MSSM as follows. Using LANHEP [60], a new CPV-MSSM model file with complex parameters was rebuilt in the CALCHEP [61] notation, thus specifying all relevant Feynman rules. For the Higgs sector, an effective potential was written in order to include, in a consistent way, higher-order effects [45]. Masses, mixing matrices and parameters of the effective potential are read directly from CPSUPERH [54], together with masses and mixing matrices of neutralinos, charginos and third generation sfermions. The masses of the first two generations of sfermions are computed at tree level from the MSSM input parameters within MICROMEGAS. The cross sections for all annihilation and coannihilation processes are computed automatically with CALCHEP. The standard MICROMEGAS routines are used to calculate the effective annihilation cross section and the relic density of the LSP. This CPV-MSSM version of MICROMEGAS was first presented in [53].

EDM constraint

We have also implemented the constraints originating from the electric dipole moment of the electron (eEDM), $d_e < 2.2 \times 10^{-27}$ e cm [55]. In the MSSM, for small to intermediate values of $\tan\beta$, the dominant contribution to d_e originates from one-loop chargino/sneutrino and neutralino/selectron exchange diagrams [62,63]. At one loop, the expression for d_e depends on the complex parameters in the neutralino/chargino sector (M_1, μ) as well as on the trilinear coupling of the electron, A_e. Note that A_e is suppressed by a factor proportional to m_e and is completely negligible for cross-section calculations. It is, however, relevant for the eEDM since d_e is itself proportional to the electron mass. The eEDM features a strong dependence on μ because the necessary helicity flip originates from the coupling of the electron to the Higgsino, which is proportional to μ. The one-loop contributions to the eEDM basically restrict ϕ_μ to $|\sin\phi_\mu| \sim \mathcal{O}(10^{-2})$ with sfermions at the TeV scale. The restrictions on the phases ϕ_1 and ϕ_e are more modest. At one loop, the eEDM constraint can be most easily evaded by raising the masses of the sfermions of the first generation, say to 10 TeV. However, for such high sfermion masses, two-loop contributions [64,65] can also become important, especially if $A_{t,b}$ and μ are also in the TeV range. Two-loop contributions are further enhanced for small values of the charged Higgs mass and for large $\tan\beta$ [66]. In the scenarios which we consider here, we will sometimes have to rely on a cancellation between one- and two-loop contributions to have an acceptable value for the eEDM.

IV. RESULTS

We now turn to the numerical analysis and present results for various scenarios for which the relic density is in agreement with WMAP. We impose grand unified theory (GUT) relations for the gaugino masses, $M_1{:}M_2{:}M_3 \approx 1{:}2{:}6$, unless mentioned otherwise. In order to satisfy the eEDM constraint, we assume in most cases that the sfermions of the first and second generation are heavy, $m_{\tilde{f}_{L,R}} =$ 10 TeV, allowing only the third generation to be at the TeV scale. Unless specific values are specified, we take $M_S \equiv M_{\tilde{Q}_3} = M_{\tilde{U}_3} = M_{\tilde{D}_3} = M_{\tilde{L}_3} = M_{\tilde{R}_3}$. For the trilinear couplings, we keep A_t as a free parameter, assuming $|A_f| =$ 1 TeV for all others. This is justified as the A_f with $f \neq t$ have only a very mild effect on the neutralino cross sections. However, one has to keep track of A_e because the electron EDM depends on the phase in the slepton sector. For simplicity we consider a common phase ϕ_l for all trilinear slepton couplings. In general, the parameters that will be allowed to vary are hence

$$\begin{aligned} &|M_1|, \quad |\mu|, \quad \tan\beta, \quad m_{H^+}, \\ &|A_t|, \quad M_S, \quad \phi_1, \quad \phi_\mu, \quad \phi_t, \quad \phi_l. \end{aligned} \tag{26}$$

As mentioned above, the eEDM will constrain ϕ_μ to ~ 0 or 180°. From now on we drop the $||$ for simplicity of notation, i.e. $|M_1|e^{i\phi_1} \to M_1 e^{i\phi_1}$, etc. So when specifying the value of a complex parameter, we implicitly mean its absolute value.

The cross sections for the annihilation and coannihilation processes will depend on phases, and so will the thermally averaged cross section $\langle \sigma v \rangle$, Eq. (21). Part of this is due to changes in the physical masses, leading to huge variations in the relic density especially when coannihilation processes are important or when annihilation occurs near a resonance. We will therefore take special care to disentangle the effects from kinematics and couplings. Indeed, as we will see, in many cases a large part of the phase dependence can be explained by changes in the masses of the involved particles. However, in some cases disentangling the kinematic effects will also lead to an enhancement of the phase dependence.

The scenarios which we consider are the typical scenarios for neutralino annihilation: the mixed b-ino–Higgsino LSP that annihilates into gauge bosons, the rapid annihilation through a Higgs resonance, coannihilation with third generation sfermions, and finally a scenario with a mixed b-ino–W-ino LSP. The case of t-channel exchange of light sfermions is discussed together with the sfermion coannihilation.

A. The mixed b-ino–Higgsino LSP

We start with the case that all scalars except the light Higgs are heavy, $M_S = m_{H^+} = 1$ TeV. In this scenario we do not expect a dependence of the relic density on the phase of the slepton sector; we therefore set $\phi_l = \phi_t$. In the real MSSM, a b-ino-like LSP with a mass of the order of 100 GeV needs a Higgsino admixture of roughly 25%–30% for its relic density to be within the WMAP range [14,67,68]. In terms of fundamental MSSM parameters this means $M_1 \approx \mu$. The main annihilation mechanisms then are $\tilde{\chi}_1^0 \tilde{\chi}_1^0 \to WW$ and ZZ through t-channel chargino and neutralino exchange, as well as $\tilde{\chi}_1^0 \tilde{\chi}_1^0 \to t\bar{t}$ when kinematically allowed. The latter proceeds through s-channel Z or h_1 exchange. The LSP Higgsino fraction determines the size of the annihilation cross section because it directly enters the $\tilde{\chi}_1^0 \tilde{\chi}_i^\pm W^\mp$ and $\tilde{\chi}_1^0 \tilde{\chi}_j^0 Z$ vertices.

We perform a scan in the M_1-μ plane and display in Fig. 1(a) the region where the relic density is in agreement with the 2σ WMAP bound, Eq. (1). In the real MSSM, when all phases are zero, only the narrow blue (dark gray) band is allowed. This band shifts slightly for negative values of μ ($\phi_\mu = 180°$). The onset of the $t\bar{t}$ annihilation channel appears as a kink. When allowing all phases to vary arbitrarily, keeping only those points for which all constraints are satisfied for at least one combination of phases, the allowed band becomes much wider; see the green (light gray) band in Fig. 1(a). For a given M_1, the allowed range for μ increases roughly from $\delta\mu \sim 10$ GeV to $\delta\mu \sim 50$ GeV. Since the eEDM constraint results in ϕ_μ close to zero or 180°, this is actually mostly due to ϕ_1. In fact, the left boundary of the green band roughly corresponds to the contour of $\Omega h^2 = 0.0945$ for $\phi_1 = \phi_\mu = 180°$.

In Fig. 1(b), we show the relative mass difference between the lightest chargino and the LSP, $\Delta m_{\tilde{\chi}_1^0 \tilde{\chi}_1^+}/m_{\tilde{\chi}_1^0} = (m_{\tilde{\chi}_1^\pm} - m_{\tilde{\chi}_1^0})/m_{\tilde{\chi}_1^0}$, in the WMAP-allowed bands of Fig. 1(a). As a general feature, $\Delta m_{\tilde{\chi}_1^0 \tilde{\chi}_1^+}/m_{\tilde{\chi}_1^0}$ decreases

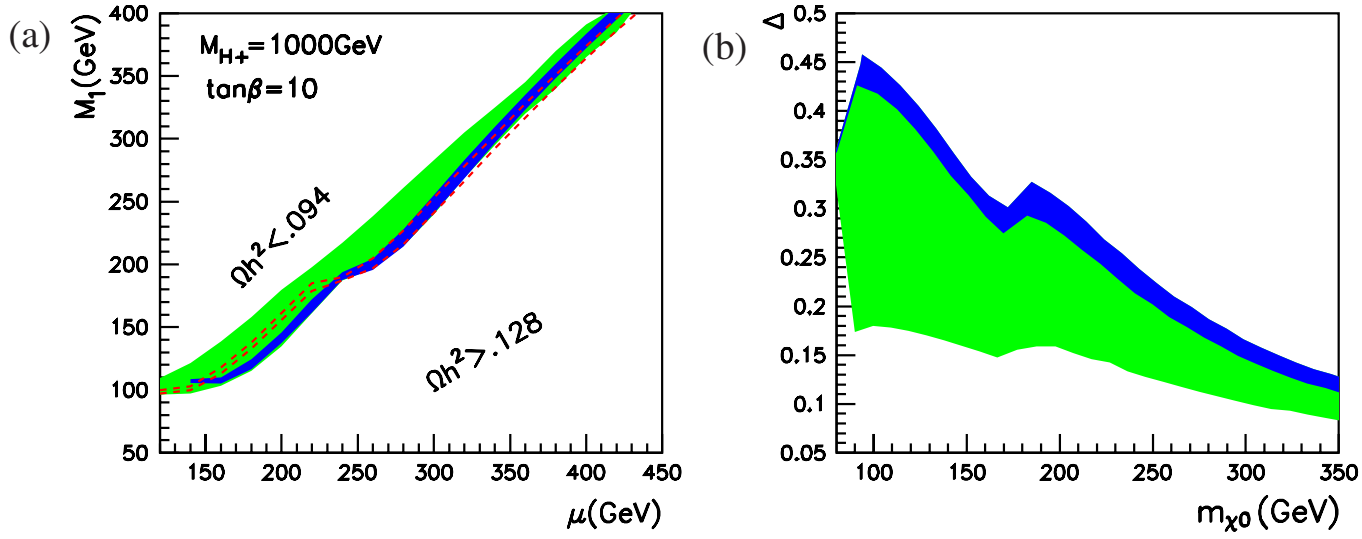

FIG. 1 (color online). (a) The 2σ WMAP bands in the M_1-μ plane for $\tan\beta = 10$, $m_{H^+} = M_S = A_t = 1$ TeV, for all phases zero (blue/dark gray band), for $\phi_\mu = 180°$ (or $\mu < 0$) and all other phases zero (dashed red lines), and for arbitrary phases (green/light gray band). (b) The corresponding relative mass difference $\Delta = \Delta m_{\tilde{\chi}_1^0 \tilde{\chi}_1^+}/m_{\tilde{\chi}_1^0}$ as a function of $m_{\tilde{\chi}_1^0}$ in the 2σ WMAP band for all phases zero (blue/dark gray band) and for arbitrary phases (green/light gray band).

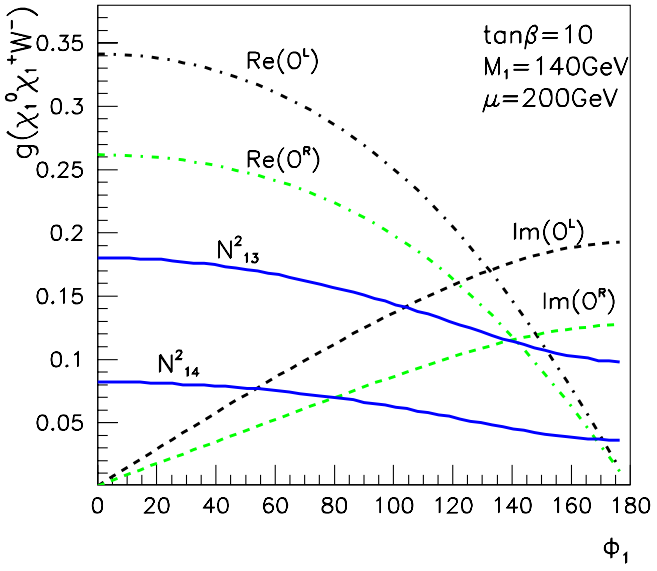

FIG. 2 (color online). The $\tilde{\chi}_1^0\tilde{\chi}_1^+W^-$ couplings, $O_{11}^{L,R}$, Eq. (9), as a function of ϕ_1, for $M_1 = 140$ GeV, $\mu = 200$ GeV, $\phi_\mu = \phi_t = 0$, and the other parameters as in Fig. 1. The Higgsino fractions of the LSP, $|N_{13}|^2$ and $|N_{14}|^2$, are also displayed.

with increasing $m_{\tilde{\chi}_1^0}$ because the cross sections for the pair-annihilation channels decrease, and coannihilation channels are needed in addition to maintain $\Omega h^2 \sim 0.1$. In the CPV-MSSM, however, for a given $m_{\tilde{\chi}_1^0}$ much smaller mass differences can be in agreement with the WMAP bound than in the *CP*-conserving case. This is because, as we will discuss in more detail below, the $\tilde{\chi}_1^0\tilde{\chi}_1^\pm W^\mp$ couplings decrease with increasing ϕ_1, so that additional contributions of coannihilation channels are required to maintain compatibility with WMAP. The phase dependence of the $\tilde{\chi}_1^0\tilde{\chi}_1^\pm W^\mp$ couplings is shown in Fig. 2 for $M_1 = 140$ GeV and $\mu = 200$ GeV.

1. Below the $t\bar{t}$ threshold

Figure 3 shows the WMAP band in the M_1-ϕ_1 plane ($\phi_\mu = \phi_t = \phi_l = 0$) for $\mu = 200$ GeV and the other parameters as above. Also shown are contours of constant LSP mass, contours of the constant LSP Higgsino fraction f_H, as well as contours of constant cross sections for the main annihilation channels. We can make several observations. First, the mass of the LSP increases with ϕ_1. On the one hand, this induces a decrease in the LSP pair-annihilation cross sections. On the other hand, since the chargino mass is independent of ϕ_1, the NLSP-LSP mass splitting is reduced, making coannihilation processes with $\tilde{\chi}_1^+$ (and also $\tilde{\chi}_2^0$) more important. Second, the Higgsino fraction decreases with increasing ϕ_1. The left- and right-handed $\tilde{\chi}_1^0\tilde{\chi}_1^\pm W^\mp$ couplings feature the same phase dependence; see Fig. 2. The modification of the LSP couplings to gauge bosons leads to a decrease in the dominant $\tilde{\chi}_1^0\tilde{\chi}_1^0 \to WW/ZZ$ cross sections and thus a higher value for the relic density. Here note that the phase dependence of f_H (and hence of the couplings) is much more pronounced than that of the LSP mass. As a result, in Fig. 3(a) there is an almost perfect match between the 2σ WMAP band and the band

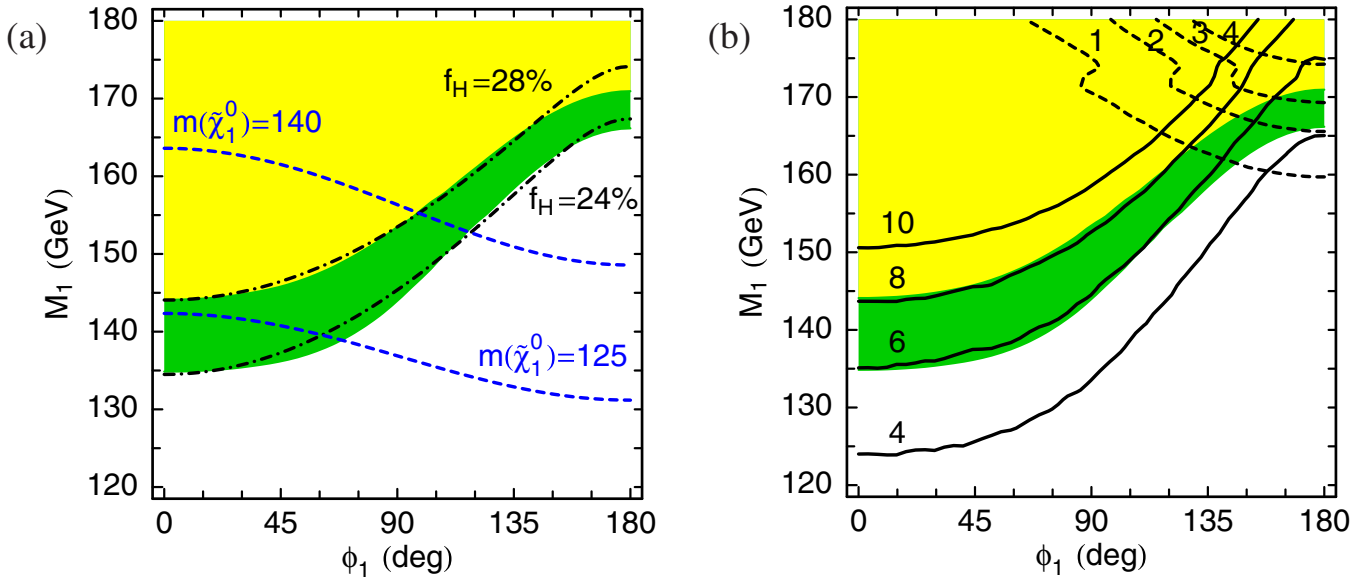

FIG. 3 (color online). The 2σ WMAP band (green/dark gray) in the M_1-ϕ_1 plane for $\mu = 200$ GeV, $\tan\beta = 10$, $m_{H^+} = 1$ TeV, $A_t = 1.2$ TeV, $\phi_t = \phi_\mu = 0$. In the yellow (light gray) region Ωh^2 is below the WMAP bound, and in the white region it is too large. Superimposed are (a) contours of constant LSP mass, $m_{\tilde{\chi}_1^0} = 125$ and 140 GeV (dashed lines) and contours of the constant LSP Higgsino fraction, $f_H = 24\%$ and 28% (dash-dotted lines) and (b) contours of constant $(\omega_{ij;kl}h^2)^{-1}$, Eq. (25), are shown; the solid lines are for $\tilde{\chi}_1^0\tilde{\chi}_1^0 \to W^+W^-$, ZZ and the dashed lines for $\tilde{\chi}_1^0\tilde{\chi}_1^\pm$ coannihilation channels.

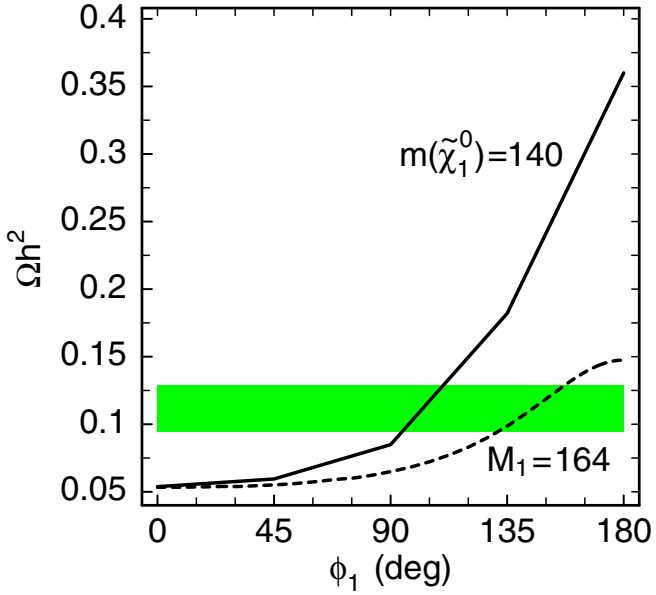

FIG. 4 (color online). Ωh^2 as a function of ϕ_1 for the parameters of Fig. 3; the dashed line is for fixed $M_1 = 164$ GeV, while for the solid line M_1 is adjusted such that $m_{\tilde{\chi}_1^0} = 140$ GeV. The green (gray) band shows the 2σ WMAP-allowed range.

of $24\% \leq f_H \leq 28\%$. The small deviation at $\phi_1 \sim 40°$–$90°$ comes from the subdominant annihilation into Zh_1 and h_1h_1. The larger deviation at $\phi_1 \sim 150°$–$180°$ comes from coannihilations; c.f. Fig. 3(b).

These features also explain why in Fig. 1(a) nonzero phases only extend the WMAP-allowed range into the region where $\Omega h^2 < 0.094$ in the real case, and not into the one where Ωh^2 is too large. Moreover, note that the phase dependence is large when annihilation into gauge bosons dominates, but weakened by contributions from coannihilation processes.

To isolate the effect that comes solely from modifications in couplings, we display in Fig. 4 the variation of Ωh^2 as a function of ϕ_1 for constant $m_{\tilde{\chi}_1^0} = 140$ GeV. For comparison, the variation of Ωh^2 for $M_1 = 164$ GeV (leading to $m_{\tilde{\chi}_1^0} \simeq 140$ GeV at $\phi_1 = 0$) is also shown. In this example, Ωh^2 varies by a factor of 3 for constant M_1, and by a factor of 7 for constant LSP mass. Overall, we find a phase dependence in Ωh^2 of almost an order of magnitude for constant LSP mass. We emphasize that, in this case of a mixed b-ino–Higgsino LSP, the dependence of masses and couplings on ϕ_1 work against each other, so that taking out the kinematic effects actually enhances the variation of Ωh^2.

2. Above the $t\bar{t}$ threshold

In the parameter range of Figs. 3 and 4 one is always below the $t\bar{t}$ threshold. We therefore consider in the next example a higher value of μ, such that $\tilde{\chi}_1^0\tilde{\chi}_1^0 \to t\bar{t}$ contributes in the WMAP-allowed region. Analogous to Fig. 3, Fig. 5 shows the WMAP band in the M_1-ϕ_1 plane for $\mu = 350$ GeV together with contours of the constant LSP mass, Higgsino fraction, and main (co)annihilation cross sections. As can be seen in Fig. 5(b), $\tilde{\chi}_1^0\tilde{\chi}_1^0 \to WW/ZZ$ and $\tilde{\chi}_1^0\tilde{\chi}_1^0 \to t\bar{t}$ are of comparable importance, each contribut-

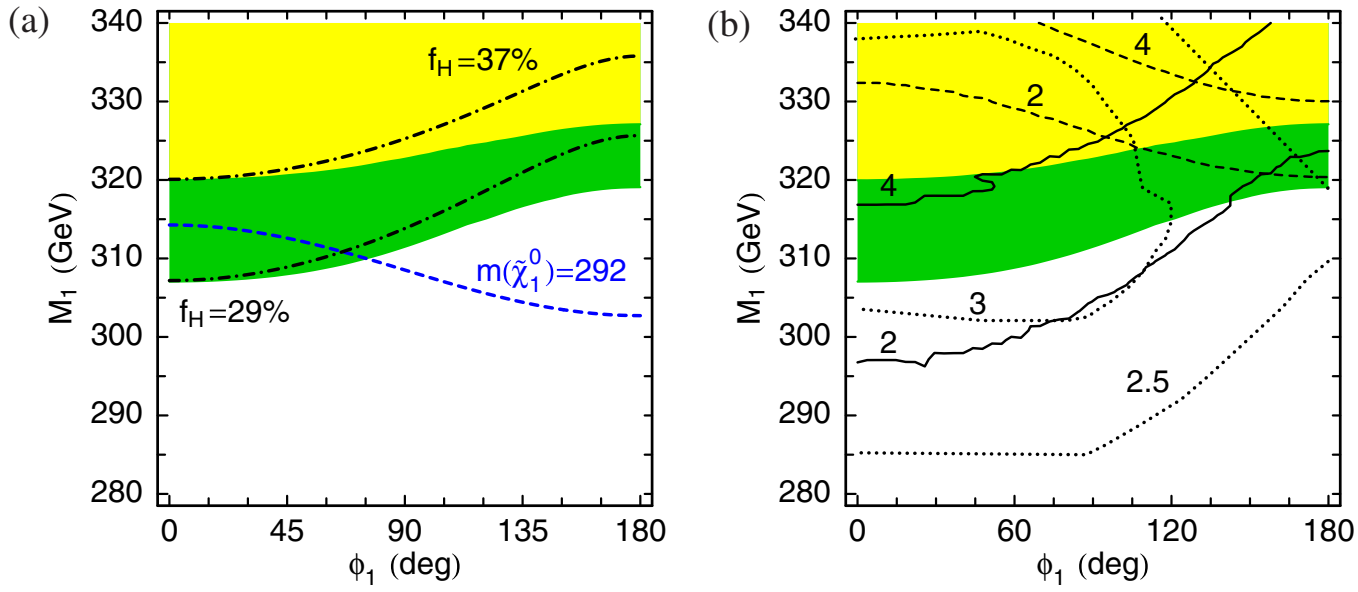

FIG. 5 (color online). The 2σ WMAP band (green/dark gray) in the M_1-ϕ_1 plane for $\mu = 350$ GeV, $\tan\beta = 10$, $m_{H^+} = 1$ TeV, $A_t = 1.2$ TeV, $\phi_t = \phi_\mu = 0$. In the yellow (light gray) region, $\Omega h^2 < 0.0945$. Superimposed are (a) a contour of constant LSP mass $m_{\tilde{\chi}_1^0} = 292$ GeV (dashed line) and contours of the constant LSP Higgsino fraction $f_H = 29\%$ and 37% (dash-dotted lines), and (b) contours of constant $(\omega_{ij;kl}h^2)^{-1}$; solid lines: $\tilde{\chi}_1^0\tilde{\chi}_1^0 \to WW/ZZ$; dashed lines: coannihilation with $\tilde{\chi}_1^+$ and $\tilde{\chi}_2^0$; dotted lines: $\tilde{\chi}_1^0\tilde{\chi}_1^0 \to t\bar{t}$.

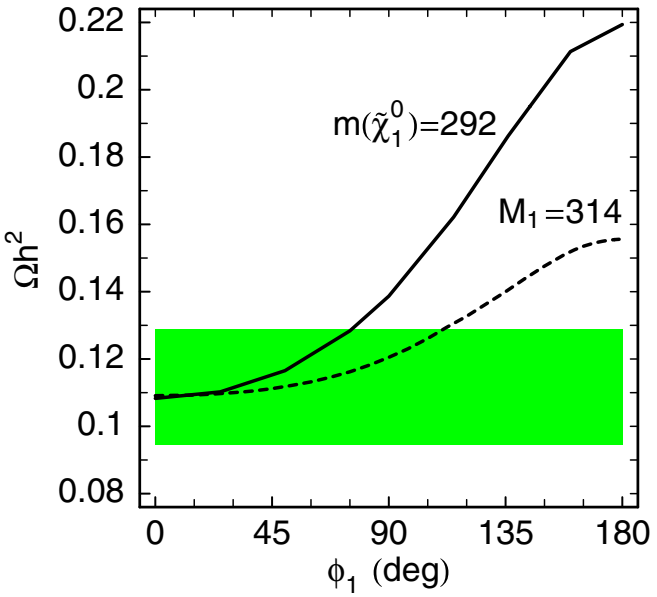

FIG. 6 (color online). Ωh^2 as a function of ϕ_1 for the parameters of Fig. 5; the dashed line is for fixed $M_1 = 314$ GeV, while for the solid line M_1 is adjusted such that $m_{\tilde{\chi}_1^0} = 292$ GeV. The green (gray) band shows the 2σ WMAP-allowed range.

ing about 40%–50% to the total annihilation cross section. The top-pair channel, proceeding through s-channel Z or h_1 exchange, shows a milder phase dependence (s-channel $h_{2,3}$ and t-channel stop exchange are negligible for this choice of parameters). Were it not for coannihilations, the lines of constant Ωh^2 would again follow the lines of constant f_H in Fig. 5(a). However, since we are now dealing with a much heavier LSP, we also need a larger Higgsino fraction to obtain the right relic density. At $\phi_1 = 0$, this means $f_H \simeq 29\%$–37%. This means, in turn, a smaller difference between M_1 and μ and hence a smaller $\tilde{\chi}_1^0 - \tilde{\chi}_1^+$ mass difference in the WMAP-allowed band as compared to the previous case. Therefore $\tilde{\chi}_1^0\tilde{\chi}_1^+$ and $\tilde{\chi}_1^0\tilde{\chi}_2^0$ coannihilations are relatively more important. Since their cross sections show the opposite phase dependence from those of the pair annihilations, and since they are mainly determined by the mass difference, the overall phase dependence of the WMAP-allowed band is much weakened.

In Fig. 6 we show the variation of Ωh^2 as a function of ϕ_1 for constant $M_1 = 314$ GeV and for constant $m_{\tilde{\chi}_1^0} = 292$ GeV. We see that, taking out kinematic effects, for a relatively heavy b-ino–Higgsino LSP the phase dependence of Ωh^2 is about a factor of 2.

3. Lowering m_{H^+} to 500 GeV

Still keeping the sfermions heavy, we next lower the charged Higgs mass to $m_{H^+} = 500$ GeV. This leads to rapid annihilation via s-channel Higgs exchange when $m_{\tilde{\chi}_1^0} \approx m_{h_i}/2 \approx 250$ GeV. In this case, only a very small coupling of the LSP to one of the Higgses (h_2, h_3) is necessary, so μ can be large and the LSP still annihilates efficiently even if it is dominantly b-ino.

In Fig. 7 we display the WMAP-allowed regions in the M_1-μ plane for both the real MSSM and the CPV-MSSM. As before, in the CPV-MSSM, the allowed region corresponds to the points in the M_1-μ plane for which there exists at least one choice of ϕ_1, ϕ_μ, ϕ_t, ϕ_l for which all constraints are satisfied. One clearly sees the two very narrow bands of the so-called Higgs funnel at $m_{\tilde{\chi}_1^0} \approx m_{H^+}/2$ and large μ. The impact of the phases on the relic density in the funnel region will be discussed in the next section. Outside this region, i.e. for small μ, we observe as before a significant widening of the band consistent with WMAP for nonzero phases. Furthermore, for $\phi_\mu \neq 0$, lower values of μ give $m_{\tilde{\chi}_1^\pm} > 103.5$ GeV, consistent with the LEP constraint [69] on charginos. This widening of the WMAP band is again due to shifts in couplings and masses as we have discussed above. Again, the widening is into the region where $\Omega h^2 < 0.0945$ in the CP-conserving case. Here note that for $M_1 = 200$ GeV the extra allowed region to the right of the blue (dark) band corresponds to $\phi_\mu = 180°$.

The shifts in masses are especially relevant in the region around the Higgs funnel. For example, at $M_1 = 270$ GeV, the band of allowed values for μ increases from 15 to 160 GeV when allowing for arbitrary phases. Here one is still close enough to the resonances to have dominant annihilation through Higgs exchange, and small changes in the $h_{2,3}$ masses have a large effect on Ωh^2. Furthermore,

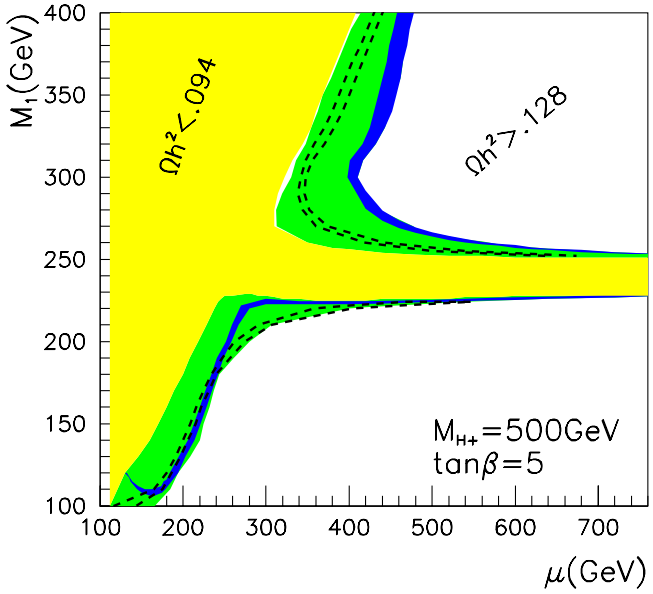

FIG. 7 (color online). The 2σ WMAP bands in the M_1-μ plane for $m_{H^+} = 500$ GeV, $A_t = 1.2$ TeV, and $\tan\beta = 5$ for all phases zero (blue/black bands) and for arbitrary phases (green/light gray bands). The other parameters are as in Fig. 1. In the yellow region, $\Omega h^2 < 0.094$. The dashed lines show contours of $\Omega h^2 = 0.094$, 0.128 when $\phi_\mu = 180°$, $\phi_1 = 0$.

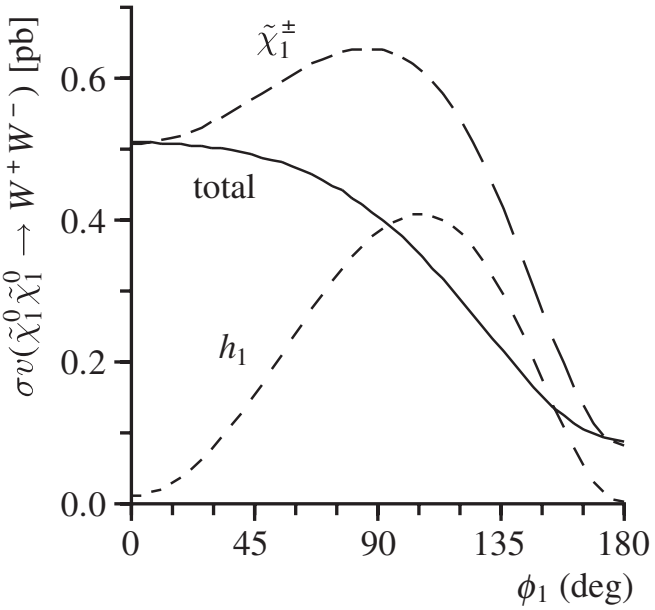

FIG. 8. Cross section times relative velocity, $\sigma v(\tilde{\chi}_1^0\tilde{\chi}_1^0 \to W^+W^-)$, as a function of ϕ_1 for $p = 10$ GeV, $M_1 = 220$ GeV, $\mu = 260$ GeV, $A_t = 1$ TeV, and the other parameters as in Fig. 7. The long-dashed line is the $\tilde{\chi}_1^\pm$ exchange, the short-dashed line the h_1 exchange, and the solid line the total contribution. Here p is the center-of-mass momentum and $v = 2p/m_{\tilde{\chi}_1^0}$.

because the couplings of the LSP to the heavy Higgses can be suppressed, in the CPV-MSSM the LSP can have a much larger Higgsino component as compared to the real case and still be in agreement with WMAP.

A priori one could think that in this region, where several channels contribute to the LSP annihilation, the impact of the shifts in couplings could be amplified by interference effects, leading to a significant impact on the effective annihilation cross section. Although we do find interference effects, they have little influence on the WMAP-allowed bands shown in Fig. 7. In fact, contrary to what was originally reported in [70], the interference effects between the s-channel Higgs and t-channel chargino exchange diagrams for $\tilde{\chi}_1^0\tilde{\chi}_1^0 \to W^+W^-$ are destructive, so that an enhancement of the cross section in one channel is largely cancelled by the other channel. An example for such an interference between the t-channel $\tilde{\chi}_1^\pm$ and s-channel h_1 exchange diagrams is shown in Fig. 8.

B. Annihilation through Higgs

In the Higgs sector, nonzero phases, in particular ϕ_t, can induce scalar-pseudoscalar mixing as well as important changes in the masses. One can therefore expect large differences between the real and complex MSSM in the Higgs-funnel region.

At vanishing relative velocity, $v \to 0$, neutralino annihilation through s-channel scalar exchange is p-wave suppressed; the annihilation proceeds strictly through pseudoscalar exchange. Nevertheless, when performing the thermal averaging, the scalar exchange cannot be neglected altogether. In the MSSM with real parameters it can amount to $\mathcal{O}(10\%)$ of the total contribution. In the presence of phases, all the neutral Higgs bosons can acquire a pseudoscalar component (that is, $g^P_{h_i\tilde{\chi}_1^0\tilde{\chi}_1^0} \neq 0$) and hence significantly contribute to neutralino annihilation even at small v. There is a kind of sum rule that relates the couplings squared of the Higgses to neutralinos. Therefore, for the two heavy eigenstates which are, in general, close in mass, we do not expect a large effect on the resulting relic density from Higgs mixing alone. A noteworthy exception occurs when, for kinematical reason, only one of the resonances is accessible to neutralino annihilation. That is, for example, the case when $m_{h_2} < 2m_{\tilde{\chi}_1^0} \simeq m_{h_3}$.

For the analysis of the Higgs funnel, we choose

$$\begin{aligned} M_1 &= 150 \text{ GeV}, \qquad \tan\beta = 5, \\ M_S &= 500 \text{ GeV}, \qquad A_t = 1200 \text{ GeV}. \end{aligned} \tag{27}$$

We consider the cases of small and large Higgsino mass parameters, $\mu = 500$ GeV and $\mu = 1$–2 TeV, leading to small and large mixing in the Higgs sector, respectively, for $\phi_t \neq 0$. In both cases the LSP is dominantly b-ino. As mentioned above, allowing for nonzero phases not only affects the neutralino and Higgs couplings but also their physical masses. Since the relic density is very sensitive to the mass difference $\Delta m_{\tilde{\chi}_1^0 h_i} = m_{h_i} - 2m_{\tilde{\chi}_1^0}$ [13,23], it is important to disentangle the phase effects in kinematics and in couplings. As we will see, a large part of the huge phase effects reported in Ref. [50] can actually be attributed to a change in $\Delta m_{\tilde{\chi}_1^0 h_i}$.

1. Small Higgs mixing

We fix $\mu = 500$ GeV so that there is small Higgs mixing. Moreover, we set $\phi_\mu = 0$ to avoid the eEDM constraint, and discuss the dependence on ϕ_1 and ϕ_t.

For real parameters and $m_{H^+} = 340$ GeV, we have $m_{\tilde{\chi}_1^0} = 147$ GeV, $m_{h_2} = 331.5$ GeV, $m_{h_3} = 332.3$ GeV, and $\Omega h^2 = 0.11$. In this case, h_2 is the pseudoscalar. The LSP annihilation channels are then characterized by the h_2 branching fractions, giving predominantly fermion pairs, $b\bar{b}$ (78%) and $\tau\bar{\tau}$ (10%), with a small contribution of Zh_1 (7%). When we vary the phases of A_t and/or M_1, we observe large shifts in the relic density.

First consider varying the phase ϕ_t, which affects the Higgs masses and mixings through loop effects. In this scenario with relatively small μ, the scalar-pseudoscalar mixing never exceeds 8%. In Fig. 9(a) we plot the band that is allowed by WMAP in the m_{H^+}-ϕ_t plane. One can see that the lower and upper WMAP bounds correspond to the contours of $\Delta m_{\tilde{\chi}_1^0 h_2} = 36.2$ and 38.6 GeV, respectively,

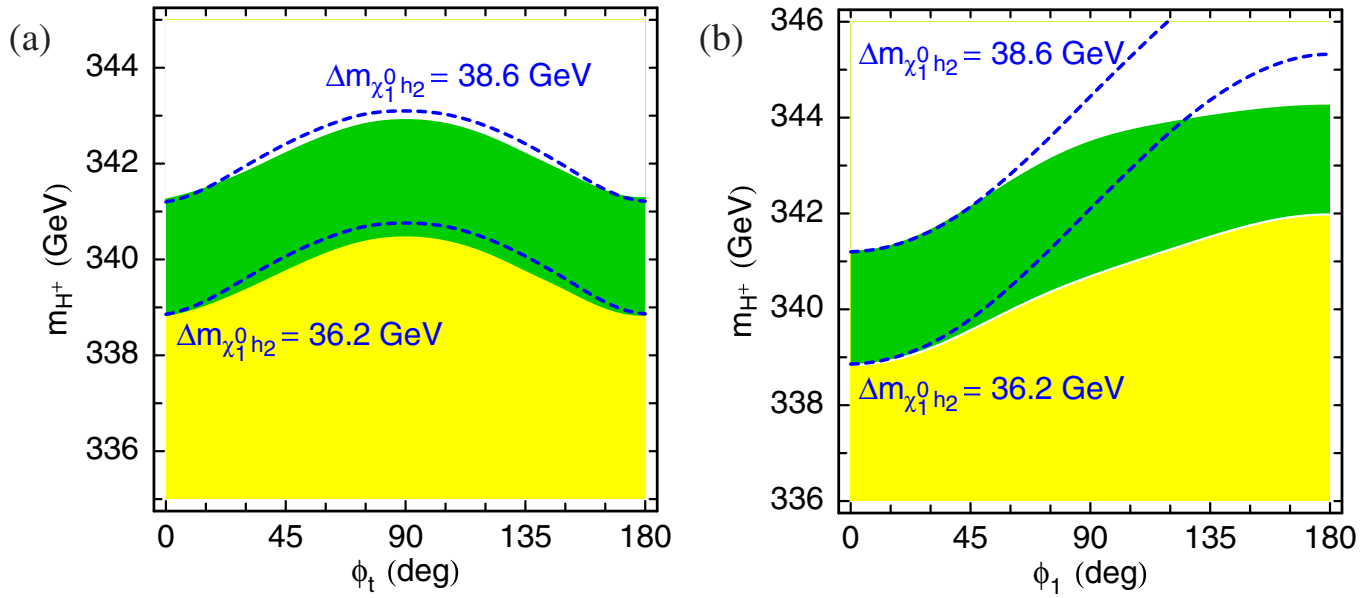

FIG. 9 (color online). The 2σ WMAP bands (green/dark gray) in the m_{H^+}-ϕ_t and m_{H^+}-ϕ_1 planes for the parameters of Eq. (27) and $\mu = 500$ GeV; $\phi_1 = 0$ in (a) and $\phi_t = 0$ in (b). Contours of constant mass differences $\Delta m_{\tilde{\chi}_1^0 h_2} = m_{h_2} - 2m_{\tilde{\chi}_1^0}$ are also displayed. In the yellow (light gray) region, Ωh^2 is below the WMAP range.

with only 4% deviation. So the main effect of ϕ_t can be explained by shifts in the physical masses and position of the resonance.

We next vary the phase ϕ_1, keeping $\phi_t = 0$. This changes the neutralino masses and mixing, and hence also the neutralino-Higgs couplings, Eq. (18). For $m_{H^+} = 340$ GeV, when increasing ϕ_1, the relic density drops; see Fig. 9(b). This is because the mass of the neutralino increases slowly, resulting in a smaller $\Delta m_{\tilde{\chi}_1^0 h_2}$. Adjusting $m_{\tilde{\chi}_1^0}$ or m_{h_2} (by changing M_1 or m_{H^+}) such that the mass difference stays constant, we find rather that the relic density increases with ϕ_1. This can be readily understood from the phase dependence of the couplings of $h_{2,3}$ to the LSP, shown in Fig. 10. For $\phi_1 = 0$, the coupling of h_2 is predominantly pseudoscalar and h_3 almost purely scalar, while for $\phi_1 = 90°$ it is h_3 that has a large pseudoscalar coupling. Therefore for $\phi_1 = 0$, h_2 exchange dominates with a large cross section, while for $\phi_1 = 90°$ one gets about equal contributions from h_2 and h_3, although with a smaller overall cross section. When increasing ϕ_1 further (up to 180°), h_2 exchange again dominates, but with a coupling to neutralinos smaller by 30% than for $\phi_1 = 0$. Thus one needs a smaller mass splitting $\Delta m_{\tilde{\chi}_1^0 h_2}$ for Ωh^2 to fall within the WMAP range; see Fig. 9(b). Moreover, for large ϕ_1 there is also a sizable contribution from $\tilde{\chi}_1^0 \tilde{\chi}_1^0 \to h_1 h_1$ with a constructive interference between s-channel h_3 and t-channel neutralino exchange. In Fig. 11 we show the variation of Ωh^2 with ϕ_1 while keeping $\Delta m_{\tilde{\chi}_1^0 h_2}$ fixed. The maximum deviation which comes purely from modifications in the couplings can reach 70%.

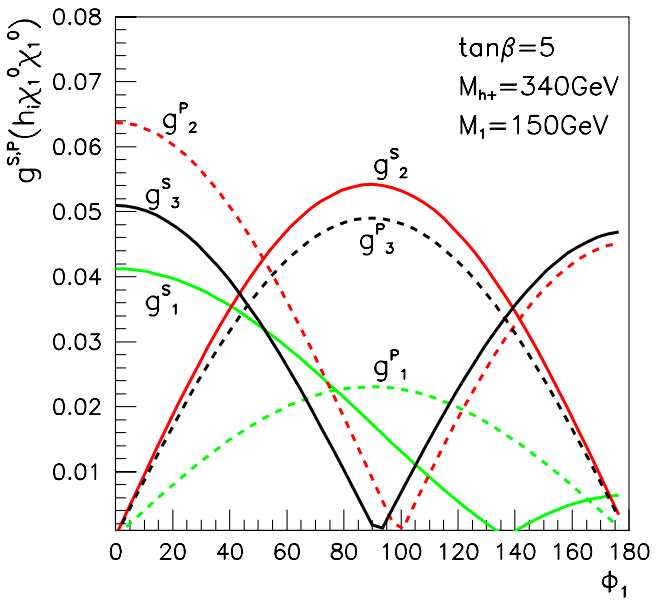

FIG. 10 (color online). The scalar (solid lines) and pseudoscalar (dashed lines) neutralino-Higgs couplings, $g^{S,P}_{h_i\tilde{\chi}_1^0\tilde{\chi}_1^0}$, as a function of ϕ_1 for $m_{H^+} = 340$ GeV, and the other parameters as in Fig. 9(b).

2. Large Higgs mixing

We next discuss the case of large mixing in the Higgs sector, which is achieved for large values of $\mu = 1$–2 TeV. For this purpose we concentrate on the ϕ_t dependence. It has to be noted that here, for large $\phi_t \approx 90°$, rather light h_i^0, and large μA_t, the EDM constraint is not satisfied by simply setting $\phi_\mu = 0$. One has to either allow for a small

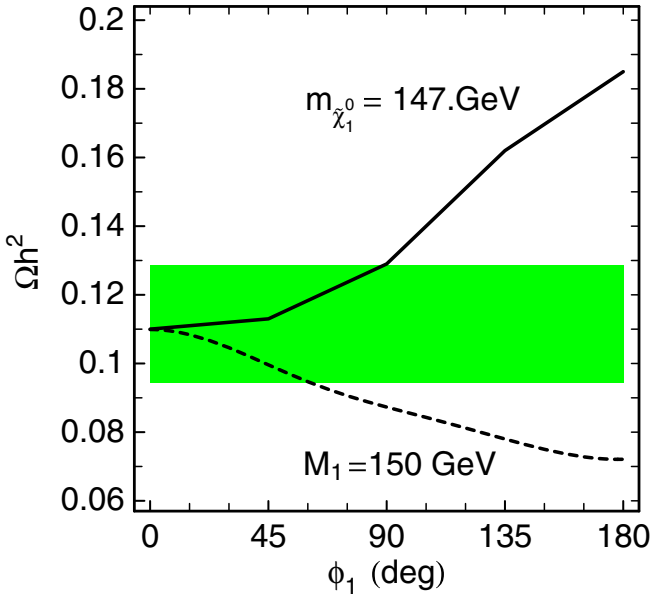

FIG. 11 (color online). Ωh^2 as a function of ϕ_1 for $m_{H^+} = 340$ GeV and the value of M_1 adjusted so that $\Delta m_{\tilde{\chi}_1^0 h_2}$ stays constant (solid line); the other parameters as in Fig. 9(b) ($m_{h_2} = 332.5$ GeV). For comparison, the variation of Ωh^2 for fixed $M_1 = 150$ GeV is shown as a dashed line. The green (gray) band corresponds to the 2σ WMAP range.

$\phi_\mu \sim \mathcal{O}(1°)$, or appeal to cancellations due to light sleptons with masses of few $\times$ 100 GeV. We choose the latter solution, imposing $\phi_\mu = 0$. Adjusting the selectron parameters such that $d_e < 2.2 \times 10^{-27}$ e cm has only a $\mathcal{O}(1\%)$ effect on the relic density in our examples.

In Fig. 12 we show the WMAP-allowed regions in the m_{H^+}-M_1 plane for this choice of parameters and maximal phase of A_t ($\phi_t = 90°$). The regions for which Ωh^2 falls within the WMAP band are shown in green (dark gray), and those for which Ωh^2 is too low in yellow (light gray). In addition, the positions of the WMAP-allowed strips for $\phi_t = 0$ are shown as dashed lines. In the *CP*-conserving case, h_3 is a pure pseudoscalar and h_2 a pure scalar, while for $\phi_t = 90°$ it is just the opposite and h_2 is dominantly pseudoscalar.

For $\mu = 1$ TeV, Fig. 12(a), the mass splitting between $h_{2,3}$ is about 10 GeV for $\phi_t = 90°$, as compared to about 2 GeV for $\phi_t = 0$. Masses and pseudoscalar contents, H_{3i}^2, of $h_{2,3}$ are depicted in Fig. 13 as a function of ϕ_t. Here note that it is h_2, i.e. the state which changes from scalar to pseudoscalar with increasing ϕ_t, which shows the more pronounced change in mass; the crossovers of 50% scalar-pseudoscalar mixing of $h_{2,3}$ occur at $\phi_t \sim 15°$ and 145°. For M_1 values up to 250 GeV, we therefore find in both the *CP*-conserving and the *CP*-violating cases two narrow bands where $0.094 < \Omega h^2 < 0.129$. For $\phi_t = 0$ (and also for $\phi_t = 180°$) both these bands are mainly due to pseudoscalar h_3 exchange, with one band just below and the other one above the pseudoscalar resonance. For $\phi_t = 90°$ the situation is different: in the lower WMAP-allowed band the LSP annihilates through the scalar h_3, with the pseudoscalar h_2 not accessible because $m_{h_2} < 2m_{\tilde{\chi}_1^0} \simeq m_{h_3}$, while in the upper band both h_2 and h_3 contribute (with h_2 exchange of course dominating). In between the two WMAP-allowed green (dark gray) bands one is too close to the pseudoscalar resonance and Ωh^2 falls below the WMAP bound; this holds for both $\phi_t = 0$ and $\phi_t = 90°$.

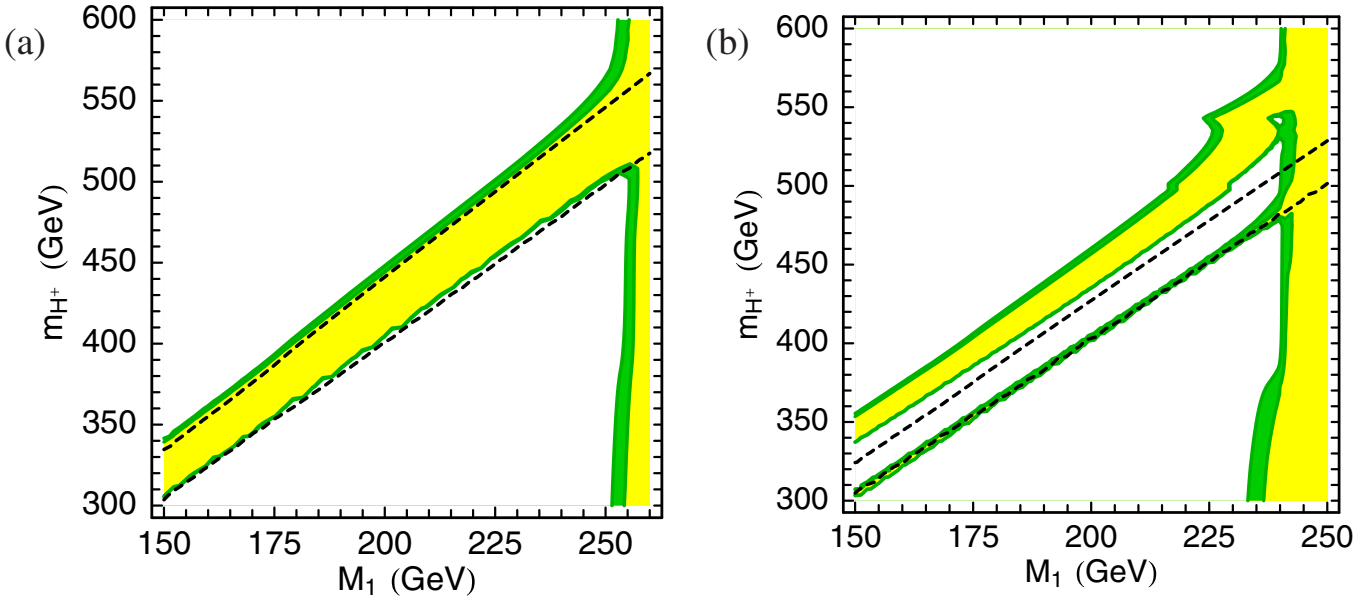

FIG. 12 (color online). The WMAP-allowed bands in the m_{H^+}-M_1 plane for (a) $\mu = 1$ TeV and (b) $\mu = 2$ TeV with $\phi_t = 90°$, $\phi_1 = 0$, and the other parameters given by Eq. (27). In the narrow green (dark gray) bands $0.0945 \leq \Omega h^2 \leq 0.1287$, while in the yellow (light gray) regions $\Omega h^2 < 0.0945$. The positions of the WMAP bands for $\phi_t = 0$ are shown as dashed lines.

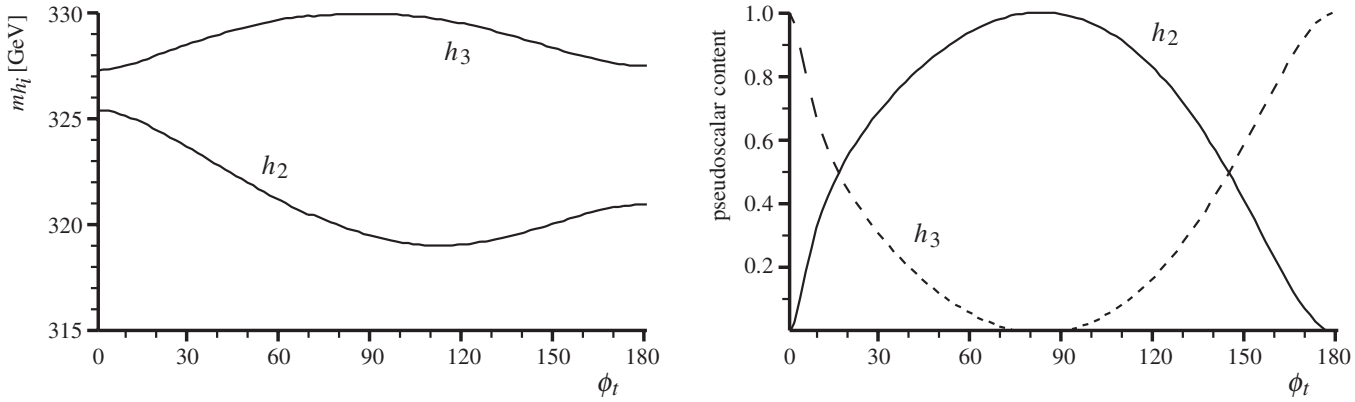

FIG. 13. Masses and pseudoscalar content of h_2 and h_3 as a function of ϕ_t for $m_{H^+} = 335$ GeV, $\mu = 1$ TeV, and the other parameters given by Eq. (27). The light Higgs has a mass of $m_{h_1} \simeq 117$ GeV and a pseudoscalar content of $\leq 10^{-4}$.

The positions of the WMAP-allowed bands for $\phi_t = 0$ and $\phi_t = 90°$ are not very different from each other. Still the difference in the relic density between $\phi_t = 0$ and $\phi_t = 90°$ is typically a factor of a few in the WMAP bands, and can reach orders of magnitudes at a pole. For $M_1 \gtrsim 250$ GeV and $\phi_t = 90°$, one enters the region of coannihilation with stops, leading to a vertical WMAP-allowed band. For $\phi_t = 0$, the $\tilde{t}_1$ is 55 GeV heavier, so the stop coannihilation occurs only at $M_1 \sim 305$ GeV (for $\phi_t = 180°$, on the other hand, $m_{\tilde{t}_1} \simeq 230$ GeV and coannihilation already sets in at $M_1 \sim 200$ GeV).

For $\mu = 2$ TeV, Fig. 12(b), there is an even stronger CP mixing of $h_{2,3}$ and the mass splitting between the two states becomes $\sim$45 GeV for $\phi_t = 90°$. The pseudoscalar contents are similar to those in Fig. 13 (right plot) with the 50% crossover at $\phi_t \sim 20°$. Moreover, because the LSP has less Higgsino admixture, one has to be closer to resonance to obtain the right relic density. As a result, the scalar and pseudoscalar funnels become separated by a region where Ωh^2 is too large [51]. In fact, the h_2 and h_3 exchange each lead to two WMAP-allowed bands, one above and one below the respective resonance. For the h_3 (scalar) exchange, however, these two regions are so close to each other that they appear as one line in Fig. 12(b). This is in sharp contrast to the CP-conserving case, $\phi_t = 0$, where the scalar and pseudoscalar states are close in mass, hence leading to only two WMAP-allowed bands. These are again shown as dashed lines in Fig. 12(b) and originate dominantly from the pseudoscalar resonance, the scalar resonance being "hidden" within.

We also display in Fig. 14 the WMAP-allowed bands for $\mu = 1$ TeV, focusing on the region of small neutralino and Higgs masses. Here we see clearly three specific Higgs annihilation funnels, each delimited by two narrow bands where Ωh^2 is within the WMAP bound. The band corresponding to h_1 exchange is also found in the CP-conserving case. However, in the CP-conserving case the LEP limit [35] on the Higgs mass, $m_{h^0} > 114$ GeV, requires $m_{H^+} \gtrsim 210$ GeV, while in the CP-violating case the limit is much lower, about $m_{h_1} \gtrsim 85$ GeV [71] at $\tan\beta = 5$ and $m_t = 175$ GeV, corresponding to $m_{H^+} \gtrsim 130$ GeV. For $m_{H^+} \lesssim 190$ GeV, the bands corresponding to h_2 and h_3 exchange are clearly separated because here the mass splitting between the two states is large, about 20–36 GeV. This is to be contrasted with the real case, where the H/A mass splitting is much smaller and annihilation through the pseudoscalar always dominates.

Let us now examine the dependence on ϕ_t in more detail. For this we fix $\mu = 1$ TeV. For vanishing phases, agreement with WMAP is found for $m_{H^+} \simeq 332$–334 GeV. This value is lower than in the scenario with small Higgs mixing because the Higgsino fraction of the LSP is smaller, so one needs to be closer to the Higgs resonance. For $\phi_t \neq$

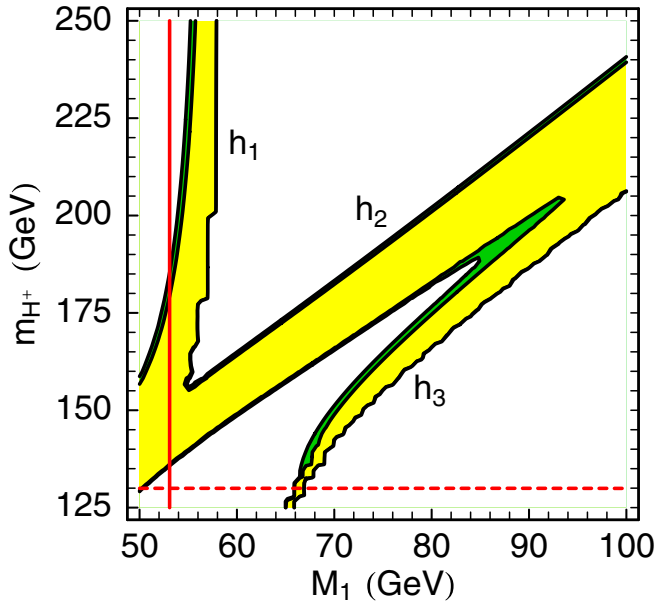

FIG. 14 (color online). Same as Fig. 12(a) but for light neutralinos and Higgs bosons. The vertical red line indicates the LEP bound on the $\tilde{\chi}_1^+$ mass, the horizontal dashed line indicates that on m_{h_1}.

0 we have a large scalar-pseudoscalar mixing and hence a stronger dependence of Ωh^2 on ϕ_t. For $\phi_t = 0$, h_3 is the pseudoscalar and gives the dominant contribution to neutralino annihilation, while for $\phi_t = 90°$, h_2 is the pseudoscalar, hence giving the dominant contribution. Consequently, in Fig. 15, agreement with WMAP is reached for $\Delta m_{\tilde{\chi}_1^0 h_i} \sim 25$ GeV with $h_i = h_3$ at $\phi_t = 0$ and 180°, and $h_i = h_2$ at $\phi_t = 90°$.

When twice the LSP mass is very near the heaviest Higgs resonance, one finds another region where the relic density falls within the WMAP range. This is shown in Fig. 15(b) [corresponding to the phase dependence of the lower WMAP-allowed band in Fig. 12(a)]. In the real case one needs $m_{H^+} = 305$ GeV, giving a mass difference $\Delta m_{\tilde{\chi}_1^0 h_3} = -1.5$ GeV. Note that annihilation is efficient enough even though one catches only the tail of the pseudoscalar resonance. For the same charged Higgs mass, the mass of h_3 increases when one increases ϕ_t, so that neutralino annihilation becomes more efficient despite the fact that h_3 becomes scalarlike and $g^P_{\tilde{\chi}_1^0 \tilde{\chi}_1^0 h_3}$ decreases. When $\phi_t \sim 75°$–$90°$, the coupling $g^P_{\tilde{\chi}_1^0 \tilde{\chi}_1^0 h_3}$ becomes very small and one needs $\Delta m_{\tilde{\chi}_1^0 h_3} = 0$–$1.5$ GeV to achieve agreement with WMAP; see Fig. 15(b). Here we are in the special case where $m_{h_2} < 2m_{\tilde{\chi}_1^0} \simeq m_{h_3}$, so that only h_3 contributes significantly to the relic density.

We can isolate the phase dependence of Ωh^2 due to the scalar-pseudoscalar mixing by keeping the distance from the h_3 pole constant. For constant values of $\Delta m_{\tilde{\chi}_1^0 h_3} = -1.5$ GeV we get an increase in Ωh^2 relative to the $\phi_t = 0$ case by almost an order of magnitude. This is, however, far less than the huge shifts of several orders of magnitude found for fixed values of m_{H^+} when a Higgs pole is passed.

C. *B*-ino-like LSP and light sfermions

In the *CP*-conserving MSSM, light sfermions can significantly contribute to reducing the relic density to a value which is in agreement with WMAP, in particular, in the case of a b-ino-like LSP. The relevant processes are $\tilde{\chi}_1^0 \tilde{\chi}_1^0 \to f\bar{f}$ via t-channel sfermion exchange, as well as coannihilation with sfermions that are close in mass to the LSP. In the CPV-MSSM with large phases, the sfermions of the first and second generations need to be heavy to avoid the EDM constraints. The third generation is, however, much less constrained and can be light. We therefore consider in this section the cases of light staus and light stops.

1. Light staus

We choose a scenario where the LSP is mostly b-ino and fix $\tan\beta = 10$, $\mu = 600$ GeV, $m_{H^+} = M_S = A_{f,t} = 1$ TeV. Moreover, we take $M_{\tilde{R}_3} = 220$ GeV and $M_{\tilde{L}_3} = 240$ GeV, so that staus are relatively light, $m_{\tilde{\tau}_1} = 212.1$ GeV, and can contribute to the neutralino annihilation. Note that for this choice of parameters there is a large mixing in the stau sector, driven by $\mu \tan\beta$. The eEDM constraint is avoided by setting $\phi_\mu = \phi_t = \phi_l = 0$. To obtain a relic density in agreement with WMAP one has to rely on stau (co)annihilation channels. For this aim, the mass difference $\Delta m_{\tilde{\chi}_1^0 \tilde{\tau}_1} = m_{\tilde{\tau}_1} - m_{\tilde{\chi}_1^0}$ must be small, in our example about 4–6 GeV. For $M_1 = 210$ GeV and

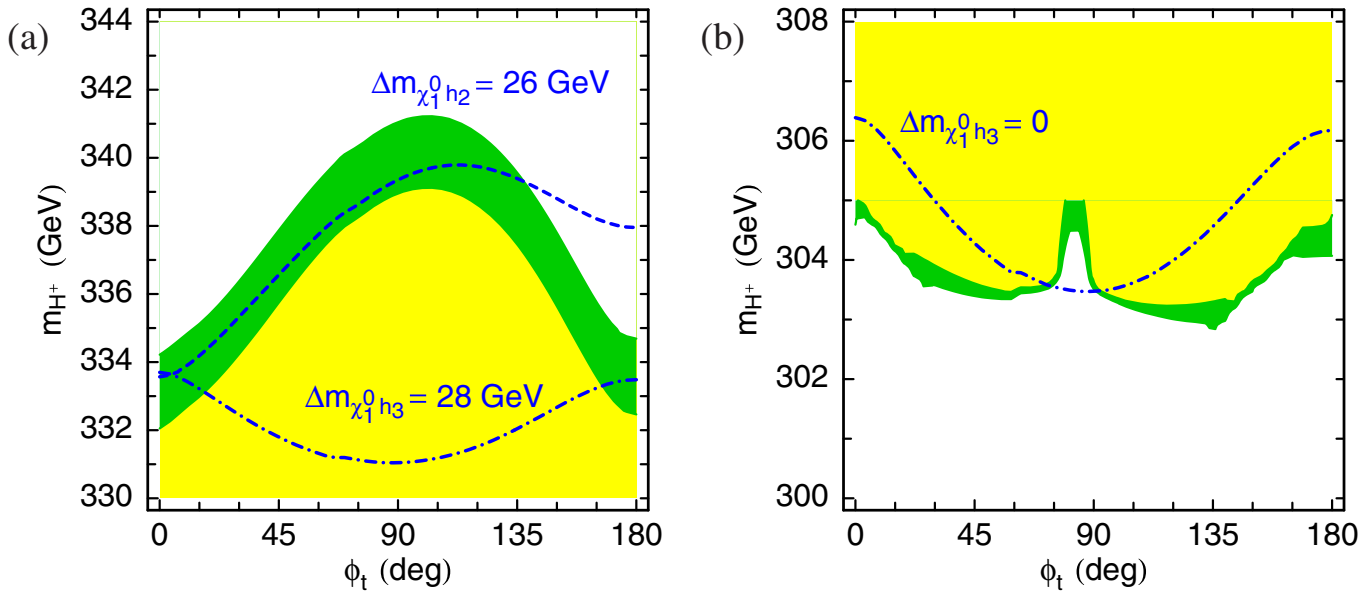

FIG. 15 (color online). The 2σ WMAP bands (green/dark gray) in the m_{H^+}-ϕ_t plane for $\mu = 1$ TeV and $m_{H^+} \sim 330$–340 GeV in (a) and $m_{H^+} \sim 305$ GeV in (b). Contours of constant mass differences $\Delta m_{\tilde{\chi}_1^0 h_i}$ are also displayed. In the yellow (light gray) region, Ωh^2 is below the WMAP range.

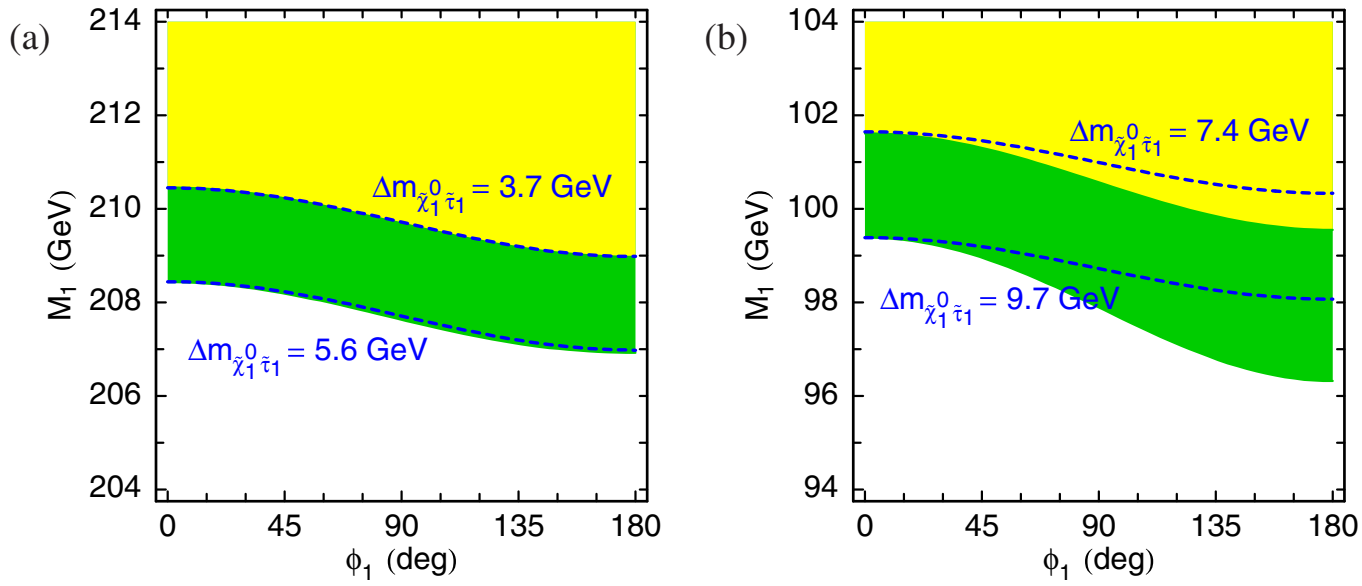

FIG. 16 (color online). The 2σ WMAP bands (green/dark gray) in the M_1-ϕ_1 plane for $m_{\tilde{\tau}_1} \simeq 212$ GeV in (a) and $m_{\tilde{\tau}_1} \simeq 108$ GeV in (b). The other parameters are given in the text. In the yellow (light gray) region, Ωh^2 is below the WMAP bound. Contours of constant mass difference $\Delta m_{\tilde{\chi}_1^0 \tilde{\tau}_1}$ are shown as dashed lines.

vanishing phases, we obtain $m_{\tilde{\chi}_1^0} = 208$ GeV, $\Delta m_{\tilde{\chi}_1^0 \tilde{\tau}_1} = 4.1$ GeV, and $\Omega h^2 = 0.102$. The main channels in this case are $\tilde{\chi}_1^0 \tilde{\tau}_1 \to \gamma\tau$ (32%), $\tilde{\chi}_1^0 \tilde{\tau}_1 \to Z\tau$ (10%), $\tilde{\tau}_1 \tilde{\tau}_1 \to \tau\tau$ (26%), and $\tilde{\tau}_1 \tilde{\tau}_1^* \to \gamma\gamma$ (12%).

It is well known that the mass difference is the key parameter in the case of coannihilations. We therefore expect large shifts in Ωh^2 for nonzero phases, resulting from small changes in the masses. Figure 16(a) shows the WMAP-allowed region in the M_1-ϕ_1 plane for the scenario given above. As can be seen, the WMAP band matches almost perfectly with the contours of constant mass difference, $\Delta m_{\tilde{\chi}_1^0 \tilde{\tau}_1} = 3.7$ and 5.6 GeV. When we adjust the parameters of the stau sector to keep a constant mass difference while varying ϕ_1, the relic density stays constant within a few percent, $\delta\Omega/\Omega \lesssim 5\%$. An analogous behavior is found for nonzero ϕ_l.

For very light neutralinos and sleptons, annihilation into lepton pairs through t-channel slepton exchange can be efficient enough to achieve $\Omega h^2 \sim 0.1$. In the mSUGRA model, this is often called the "bulk" region. Owing to the LEP limit of $m_{\tilde{l}} \gtrsim 90$–100 GeV [69] (depending on the slepton flavor and chirality/mixing and on $m_{\tilde{l}} - m_{\tilde{\chi}_1^0}$), and because the t-channel slepton contribution scales as $m_{\tilde{\chi}_1^0}^2 / m_{\tilde{l}}^4$, the bulk is squeezed into a small region of slepton masses of about 100 GeV. To investigate this case in the CPV-MSSM, we lower the stau parameters to $M_{\tilde{R}_3} = 135$ GeV, $M_{\tilde{L}_3} = 150$ GeV and $A_\tau = 100$ GeV, $\phi_l = 0$. This gives $m_{\tilde{\tau}_1} = 107.8$ GeV, $m_{\tilde{\tau}_2} = 182.1$ GeV, and $m_{\tilde{\nu}_\tau} = 135.7$ GeV. The WMAP band in the M_1-ϕ plane for this scenario is shown in Fig. 16(b). For $m_{\tilde{\chi}_1^0} \lesssim 100$ GeV, that is, up to $M_1 \sim 100$ GeV, $\tilde{\chi}_1^0 \tilde{\chi}_1^0 \to \tau^+\tau^-$ is the dominant process. For heavier neutralinos, $\tilde{\chi}_1^0 \tilde{\tau}_1$ coannihilation dominates. Agreement with WMAP is achieved for larger $\tilde{\chi}_1^0 - \tilde{\tau}_1$ mass differences than in the previous example. Since coannihilations are less important, we find a stronger phase dependence which is not completely

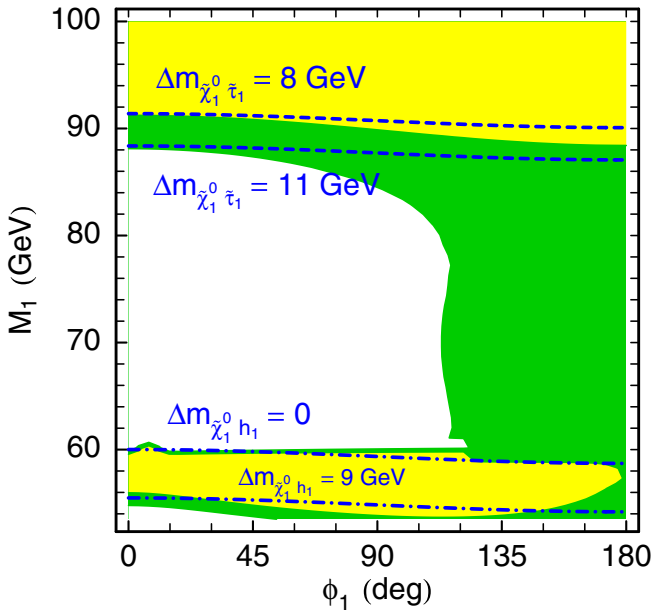

FIG. 17 (color online). The 2σ WMAP bands (green/dark gray) in the M_1-ϕ_1 plane for $m_{\tilde{\tau}_1} \simeq 98$ GeV. The other parameters are given in the text. In the yellow (light gray) region, Ωh^2 is below the WMAP bound. Also shown are contours of constant mass differences $\Delta m_{\tilde{\chi}_1^0 \tilde{\tau}_1} = m_{\tilde{\tau}_1} - m_{\tilde{\chi}_1^0}$ (dashed lines) and $\Delta m_{\tilde{\chi}_1^0 h_1} = m_{h_1} - 2m_{\tilde{\chi}_1^0}$ (dash-dotted lines).

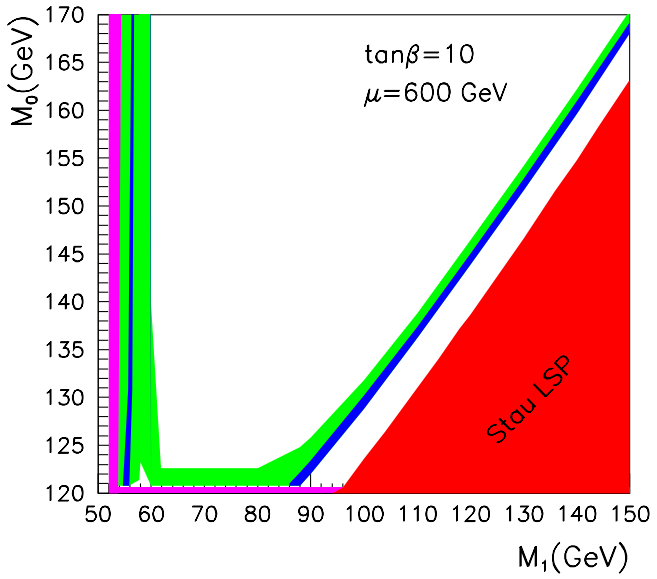

FIG. 18 (color online). The 2σ WMAP bands in the M_0-M_1 plane, with $M_0 = M_{\tilde{R}_3} = 0.9 M_{\tilde{L}_3}$; the blue (black) bands are for vanishing phases, the green (medium gray) one for arbitrary phases, ϕ_1, $\phi_t = \phi_l$. The pink (dark gray) region is excluded by the requirements $m_{\tilde{\chi}_1^\pm} > 103.5$ GeV, $m_{\tilde{\tau}_1} > 95$ GeV. In the lower right-hand corner (red/dark gray) the $\tilde{\tau}_1$ is the LSP.

determined by $\Delta m_{\tilde{\chi}_1^0 \tilde{\tau}_1}$; see Fig. 16(b). When keeping the masses constant, the maximal variation in Ωh^2 due to ϕ_1 is about 15%. Last but not least, note that s-channel Z and Higgs exchange is negligible in this scenario; t-channel exchange of $\tilde{\tau}_2$, however, does contribute and there is, in fact, a strong destructive interference between the $\tilde{\tau}_1$ and $\tilde{\tau}_2$ exchange diagrams.

Let us lower the stau mass parameters even further, close to the experimental limit while keeping $\phi_\tau = 0$. For $M_{\tilde{R}_3} = 130$ GeV, $M_{\tilde{L}_3} = 140$ GeV, we get $m_{\tilde{\tau}_1} = 98.2$ GeV, $m_{\tilde{\tau}_2} = 175.9$ GeV, and $m_{\tilde{\nu}_\tau} = 124.6$ GeV. The WMAP-allowed regions in the M_1-ϕ_1 plane for this case are shown in Fig. 17. The almost horizontal bands of annihilation through the light Higgs ($m_{h_1} = 118$ GeV) for very light $\tilde{\chi}_1^0$, as well as the stau coannihilation region at $M_1 \gtrsim 90$ GeV are clearly visible. The peculiar feature is that for a large phase, $\phi_1 \gtrsim 110°$, a new region appears, connecting the light Higgs funnel and the stau coannihilation strip, where Ωh^2 is within the WMAP bound. In this region, $\tilde{\chi}_1^0 \tilde{\chi}_1^0 \to \tau\tau$ completely dominates, and the phase dependence originates from the $\tilde{\chi}_1^0 \tilde{\tau}_{1,2} \tau$ couplings. Again, there is an important interference between the $\tilde{\tau}_1$ and $\tilde{\tau}_2$ exchange diagrams.

That this new "stau bulk" region is generic can be seen in Fig. 18. Here we plot the WMAP-allowed bands in the M_0-M_1 plane, with $M_0 \equiv M_{\tilde{R}_3} = 0.9 M_{\tilde{L}_3}$. For vanishing phases, the light Higgs funnel and $\tilde{\tau}$ coannihilation regions appear as narrow disconnected strips. For arbitrary phases ϕ_1, ϕ_μ, ϕ_t, ϕ_l, these strips are much wider; in particular, the light Higgs funnel becomes a band instead of a narrow strip. Furthermore, the Higgs funnel is connected to the $\tilde{\tau}$ coannihilation region by the t-channel stau exchange region, which appears as a horizontal band at $M_0 \sim 130$ GeV.

2. Light stops

To discuss the case of a light stop, we fix $M_{\tilde{Q}_3} = 500$ GeV, $M_{\tilde{U}_3} = 450$ GeV, $M_{\tilde{D}_3} = 800$ GeV, $\mu = M_S = m_{H^+} = 1$ TeV, and $\tan\beta = 5$. We again fix $\phi_\mu = 0$ to easily avoid the eEDM constraint. Moreover, we choose $A_t = 1$ TeV and $\phi_t = 180°$ to obtain a light $\tilde{t}_1$, $m_{\tilde{t}_1} = 243.5$ GeV. Since μ is large we are again in a scenario with a b-ino LSP. A relic density in agreement with WMAP is found for $M_1 \approx 215$ GeV ($m_{\tilde{\chi}_1^0} \approx 214$ GeV) in the real case. The main channels are $\tilde{\chi}_1^0 \tilde{\chi}_1^0 \to t\bar{t}$ (21%), $\tilde{\chi}_1^0 \tilde{t}_1 \to t h_1$ (57%), and $\tilde{\chi}_1^0 \tilde{t}_1 \to g t$ (17%). Note that $\tilde{\chi}_1^0 \tilde{t}_1$ coannihilation dominates although the mass difference is much larger than in the case of $\tilde{\chi}_1^0 \tilde{\tau}_1$ coannihilation.

The phases that can play a role here are ϕ_1 and ϕ_t. As we have already observed in other coannihilation scenarios, the relic density is extremely sensitive to the mass difference $\Delta m_{\tilde{\chi}_1^0 \tilde{t}_1} = m_{\tilde{t}_1} - m_{\tilde{\chi}_1^0}$. However, in the stop-coannihilation scenario we also observe some important effects due to the phase dependence of the couplings.

First we vary only ϕ_1 and show in Fig. 19(a) the WMAP-allowed band in the M_1-ϕ_1 plane. We find the WMAP band does not match the contours of constant mass difference $\Delta m_{\tilde{\chi}_1^0 \tilde{t}_1} = m_{\tilde{t}_1} - m_{\tilde{\chi}_1^0}$. A much larger mass difference is required at $\phi_1 = 180°$ ($\Delta m_{\tilde{\chi}_1^0 \tilde{t}_1} = 34.2$–$38.6$ GeV) then at $\phi_1 = 0$ ($\Delta m_{\tilde{\chi}_1^0 \tilde{t}_1} = 28.8$–$31.0$ GeV). The reason for this is an increase of both the $\tilde{\chi}_1^0 \tilde{\chi}_1^0 \to t\bar{t}$ as well as the $\tilde{\chi}_1^0 \tilde{t}_1 \to t h_1$ cross sections with the phase ϕ_1. For the coannihilation process, the phase dependence is enhanced by a constructive interference between the t-channel $\tilde{t}_1$ and the s-channel top exchange diagrams.

To investigate also the dependence on ϕ_t, we now fix $M_1 = 212$ GeV and $\phi_1 = 0$ ($m_{\tilde{\chi}_1^0} = 210.8$ GeV) and plot in Fig. 19(b) the WMAP-allowed band in the A_t-ϕ_t plane. The other parameters are as above. As before, agreement with WMAP is found only for a narrow band in which $\tilde{\chi}_1^0 \tilde{t}_1 \to t h_1$ dominates. Although in this band the $\tilde{t}_1$ mass is constant within 10 GeV, there is no exact match between the contours of constant Ωh^2 and $\Delta m_{\tilde{\chi}_1^0 \tilde{t}_1}$. Rather, at $\phi_t = 0$, 90°, and 180°, agreement with WMAP requires $\Delta m_{\tilde{\chi}_1^0 \tilde{t}_1} \sim 36$ GeV, 32 GeV, and 30 GeV, respectively (each about ± 2 GeV).

When keeping the mass difference constant, we can single out the phase dependence of Ωh^2 that comes solely from changes in the couplings. This is shown in Fig. 20, where we plot Ωh^2 as a function of ϕ_1 for $\phi_t = 180°$ (dashed line) and as a function of ϕ_t for $\phi_1 = 0$ (dash-

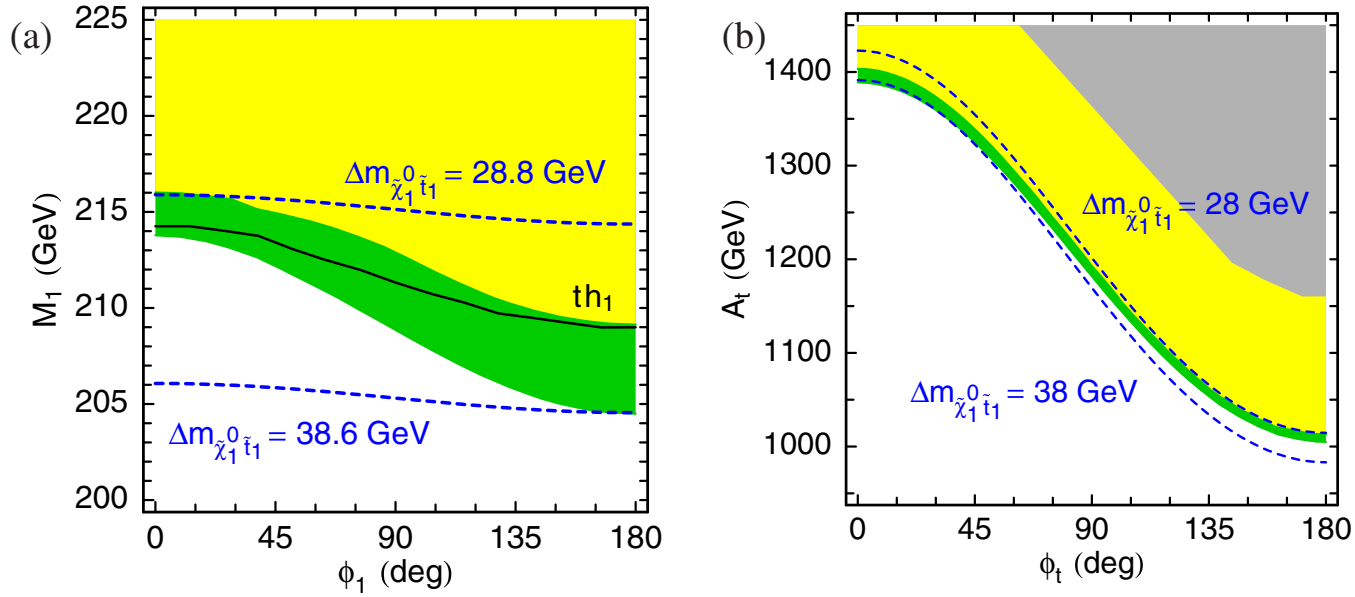

FIG. 19 (color online). The 2σ WMAP bands (green/dark gray) for the stop-coannihilation scenario, (a) in the M_1-ϕ_1 plane for $m_{\tilde{t}_1} = 243.5$ GeV and (b) in the A_t-ϕ_t plane for $m_{\tilde{\chi}_1^0} = 210.8$ GeV. The other parameters are given in the text. In the yellow (light gray) regions, $\Omega h^2 < 0.0945$. The medium gray region in (b) is theoretically excluded. Also shown are contours of constant mass difference $\Delta m_{\tilde{\chi}_1^0 \tilde{t}_1}$ (blue dashed line). The solid black line in (a) is a contour of constant $\langle \sigma v \rangle (\tilde{\chi}_1^0 \tilde{t}_1 \to t h_1)$.

dotted line), each time keeping $\Delta m_{\tilde{\chi}_1^0 \tilde{t}_1} = 32$ GeV constant by adjusting either M_1 or A_t. As can be seen, in either case Ωh^2 varies between 0.08 and 0.14. For comparison, the variation of Ωh^2 with ϕ_1 for $M_1 = 212$ GeV ($A_t = 1$ TeV, $\phi_t = 180°$), i.e. varying mass difference, is also shown.

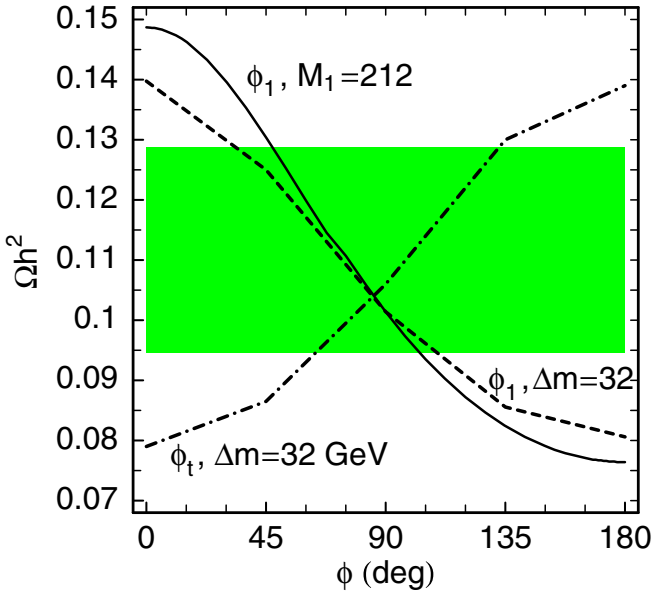

FIG. 20 (color online). Ωh^2 in the stop-coannihilation scenario as a function of ϕ_1 (dashed line) and as a function of ϕ_t (dash-dotted line) for constant mass difference $\Delta m_{\tilde{\chi}_1^0 \tilde{t}_1} = 32$ GeV. For comparison, the variation of Ωh^2 with ϕ_1 for fixed $M_1 = 212$ GeV is also shown. See text for details.

C. Relaxing the gaugino GUT relation: the *b*-ino/*W*-ino scenario

We now consider relaxing the universality condition amongst the first two gaugino mass parameters and treat M_1 and M_2 as two independent parameters. As we want to examine specifically the role of the W-ino component, we fix $\mu = 1$ TeV and $m_{H^+} = 1$ TeV, then the Higgsino component of the LSP is small and the annihilation near Higgs resonance not possible. Because we choose sfermions to be heavy, the annihilation into fermion pairs is suppressed. The LSP can hence only pair annihilate into gauge bosons.

Choosing $M_2/M_1 < 2$ increases the W-ino component of the LSP. Since the neutralino-chargino-W coupling also has a term proportional to N_{i2}, one could think that the b-ino–W-ino scenario is quite similar to the mixed b-ino–Higgsino case discussed in Sec. IV A. However, when the parameters are set such that $f_W = |N_{i2}|^2$ becomes sizable, say around 10%, the mass difference $\Delta m_{\tilde{\chi}_1^0 \tilde{\chi}_1^+}$ becomes small (few GeV), and the coannihilation channels are so important that the relic density is well below the WMAP limit, unless $M_{1,2} \sim \mathcal{O}(1)$ TeV.

In fact, in the mass range which is interesting for collider searches, the LSP still has to be overwhelmingly b-ino, and the relic density is completely dominated by coannihilation channels involving $\tilde{\chi}_1^0 \tilde{\chi}_1^\pm$, $\tilde{\chi}_1^0 \tilde{\chi}_2^0$, $\tilde{\chi}_2^0 \tilde{\chi}_1^\pm$, $\tilde{\chi}_2^0 \tilde{\chi}_2^0$, $\tilde{\chi}_1^\pm \tilde{\chi}_1^\pm$.[3] Final states involve a variety of channels from gauge boson

[3]This scenario was considered in Ref. [72] for negative values of M_1, that is, $\phi_1 = 180°$.

pairs to fermion pairs of all three generations. Even when letting all phases vary, the relic density falls within the WMAP range only for a very narrow range of parameters; for a given value of M_1 the viable range of M_2 varies by only 2–3 GeV. For $\tan\beta = 10$, for instance, the allowed band can roughly be parametrized as

$$M_2 \simeq (2.03 \times 10^{-4} M_1^2 + 1.02 M_1 + 9) \pm 2 \qquad (28)$$

with M_1 given in GeV. This is typical for scenarios that are dominated by coannihilation in the sense that only a narrow range of mass difference between the NLSP and the LSP is allowed. Furthermore, considering the large number of contributing channels, the phase dependence in each individual channel tends to be "softened." For example, for $M_2 = 200$ GeV, $M_1 = 179$ GeV, $\tan\beta = 10$, we have $\Delta m_{\tilde{\chi}_1^+ \tilde{\chi}_1^0} = 21.2$ GeV and $\Omega h^2 = 0.121$; the dominant channels are $\tilde{\chi}_2^0 \tilde{\chi}_1^+ \to f\bar{f}'$ altogether contributing around 40% of the total effective annihilation cross section. In Fig. 21, we display the WMAP-allowed range in the M_1-ϕ_1 plane for $\phi_\mu = 0$. The contours of constant Ωh^2 basically follow the contours of constant mass difference $\Delta m_{\tilde{\chi}_1^0 \tilde{\chi}_1^+}$, as expected when coannihilation channels are dominant. Only for $\phi_1 > 90°$ is there a small increase in Ωh^2 due to shifts in couplings, introducing a small gap between the contours of constant mass difference and those of constant Ωh^2. For a given $\Delta m_{\tilde{\chi}_1^0 \tilde{\chi}_1^+}$, the maximal deviation from the case of vanishing phases reaches $\Delta\Omega/\Omega \approx 25\%$.

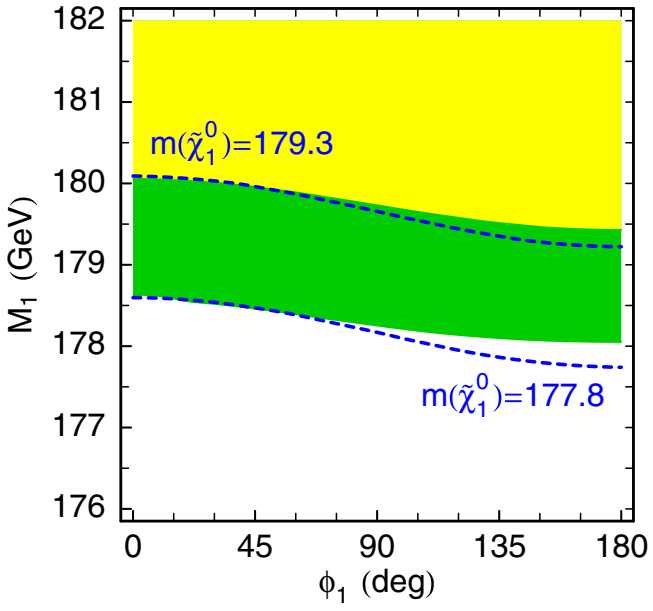

FIG. 21 (color online). The 2σ WMAP-allowed band (green/dark gray) in the M_1-ϕ_1 plane for $M_2 = 200$ GeV, $\tan\beta = 10$, $\mu = M_S = m_{H^+} 1$ TeV, $\phi_t = \phi_\mu = 0$. Superimposed are contours of constant $\tilde{\chi}_1^0$ masses (blue dashed lines). In the yellow (light gray) region, Ωh^2 is below the WMAP range.

V. SUMMARY AND CONCLUSIONS

We have performed the first complete computation of the relic density of neutralino dark matter in the CPV-MSSM, including, in a consistent manner, phases in all annihilation and coannihilation processes. Moreover, we have presented a comprehensive study of the typical scenarios that predict a relic density in agreement with WMAP. Since *CP* phases do not only change the sparticle and Higgs mixings but also the masses, we have taken care to disentangle effects from kinematics and couplings.

A priori one could think that taking out the effects which come from changes in the masses would diminish the phase dependence of Ωh^2. For processes for which the mass difference is the most important parameter, i.e. for coannihilations or annihilation near a pole, this is indeed the case. On the other hand, we have found several examples where the phase dependence of masses and couplings work against each other, and taking out the kinematic effects actually enhances the variation in Ωh^2. This happens, for instance, in the case of a mixed b-ino–Higgsino LSP, where we have found effects of almost an order of magnitude from modifications in the couplings due to nonzero *CP* phases. In the case of annihilation through s-channel Higgs exchange, for small scalar-pseudoscalar mixing, we have found cases where for fixed MSSM parameters Ωh^2 goes down with increasing ϕ_1, but when keeping the mass difference between the pseudoscalarlike Higgs pole and $2m_{\tilde{\chi}_1^0}$ constant, Ωh^2 actually goes up. This effect is of the order of 50% and dominantly due to changes in the scalar-/pseudoscalar-type coupling of the LSP. Much larger effects have been found for large scalar-pseudoscalar mixing. In the peculiar case that only one resonance is accessible to neutralino annihilation, we have found order-of-magnitude variations in Ωh^2 due to changes in the pseudoscalar content of this resonance. Moreover, in some cases we have found large interference effects in the most important annihilation or coannihilation channels. Such interferences do not, however, necessarily lead to a large variation in Ωh^2.

We have also considered scenarios with a b-ino-like LSP and light sfermions (stops and staus), and studied the phase dependence in the regions where (a) annihilation into $f\bar{f}$ dominates and (b) coannihilations dominate, as well as the intermediate region where (c) both t-channel exchange and coannihilation are important. In the stop-coannihilation region, when $\tilde{\chi}_1^0 \tilde{t}_1 \to t h_1$ is the dominant process, the variation in Ωh^2 can be about a factor of 2 due to changes in the $\tilde{\chi}_1^0 \tilde{t}_1 h_1$ couplings. There is, moreover, a constructive interference between the t-channel $\tilde{t}_1$ and the s-channel top exchange diagrams. Another peculiar feature arises for (very) light staus: here we have found a region where for large phase ϕ_1 the annihilation into $\tau\tau$ alone can be efficient enough to obtain agreement with the WMAP bound. This region does not occur for zero phases.

We emphasize that, even in scenarios which feature a modest phase dependence, once the kinematic effects are singled out, the variations in Ωh^2 are comparable to (and often much larger than) the $\sim 10\%$ range in Ωh^2 of the WMAP bound. Therefore, when aiming at a precise prediction of the neutralino relic density from collider measurements, it is clear that one does not only need precise sparticle spectroscopy—one also has to precisely measure the relevant couplings. As we have shown in this paper, this programme certainly includes the determination of possible *CP* phases. For zero phases, in a b-ino scenario with light sleptons, one may be able to infer Ωh^2 of the LSP with roughly the WMAP precision ($\sim 15\%$) from LHC measurements [73,74]. At the International Linear Collider, one expects to achieve much higher precisions, allowing for a prediction of $\Delta\Omega/\Omega$ of the level of a few percent in the case of a b-ino LSP annihilating through light sleptons [75] and in the stau coannihilation scenario [76,77]. In the b-ino–Higgsino scenario, $\Delta\Omega/\Omega \sim 15\%$ may be achieved [75]. Whether similar precisions can be reached in the CPV-MSSM requires careful investigation.

To emphasize the need to determine as completely as possible the underlying parameters of the model, we stress again that we have found examples where in the CPV-MSSM the relic density of the LSP could be quite different as compared to that in the MSSM with vanishing phases. Simply from a precise measurement of part of the mass spectrum one could be led to wrongly conclude that, for instance, the model does not give a good dark matter candidate, or else that some significant thermal production is necessary to explain the observed number density. At the same time it is important to note that a computation of $\langle\sigma v\rangle$ at next-to-leading order will be necessary to achieve the required precision in the prediction of Ωh^2; see [78–80]. Last but not least, we stress that, in addition, direct or indirect detection of the CDM candidate will be indispensable to pin down the dark matter in the Universe.

Finally we remark that we have not taken into account the constraint arising from $b \to s\gamma$. The supersymmetric corrections to the branching ratio for $b \to s\gamma$ depend mostly on the squark and gaugino/Higgsino sector as well as on the charged Higgs. In the real MSSM, large corrections are found at large values of $\tan\beta$, which we do not consider in this paper. Large corrections might also arise in scenarios with a light charged Higgs. A detailed study of the impact of this measurement in the CPV-MSSM is left for a future work.

ACKNOWLEDGMENTS

We thank T. Gajdosik and W. Porod for comparisons in the CPV-MSSM and J. S. Lee for his help with CPSUPERH. We also thank S. Y. Choi for discussions. This work was supported in part by GDRI-ACPP of CNRS and by grants from the Russian Federal Agency for Science, No. NS-1685.2003.2 and No. RFBR-04-02-17448. S. K. is supported by an APART (Austrian Programme for Advanced Research and Technology) grant of the Austrian Academy of Sciences. A. P. acknowledges the hospitality of CERN and LAPTH where some of the work contained here was performed.

Note added.—While this paper was in preparation, the WMAP Collaboration published new results corresponding to three years of data taking. The new WMAP + SDSS combined value for the relic density of dark matter is $\Omega_{\rm CDM}h^2 = 0.111^{+0.006}_{-0.011}$ at 1σ [81]. This is only slightly below the value used in this paper, so our conclusions do not change with the new data.

APPENDIX: INTERACTION LAGRANGIAN

We here give the relevant sparticle interactions with other sparticles and SM particles in the CPV-MSSM. The Higgs boson interactions with sparticles and particles can be found in [54].

1. Neutralino-neutralino-Z

Neutralinos couple to Z bosons via their Higgsino components:

$$\mathcal{L}_{\tilde{\chi}^0\tilde{\chi}^0 Z} = \frac{g}{4c_W} Z_\mu \bar{\tilde{\chi}}_i^0 \gamma^\mu (O''^L_{ij} P_L + O''^R_{ij} P_R) \tilde{\chi}_j^0 \qquad \text{(A1)}$$

with $i, j = 1, \ldots, 4$, $P_{L,R} = \frac{1}{2}(1 \mp \gamma^5)$ and

$$O''^L_{ij} = (N_{i4}N^*_{j4} - N_{i3}N^*_{j3}) = -O''^{R*}_{ij}. \qquad \text{(A2)}$$

One can also write Eq. (A1) as

$$\mathcal{L}_{\tilde{\chi}^0\tilde{\chi}^0 Z} = \frac{g}{4c_W} Z_\mu \bar{\tilde{\chi}}_i^0 \gamma^\mu [i\,\mathrm{Im}(O''^L_{ij}) + \mathrm{Re}(O''^L_{ij})\gamma^5] \tilde{\chi}_j^0. \qquad \text{(A3)}$$

2. Chargino-chargino-Z, γ

The interaction of two charginos with electroweak gauge bosons is

$$\mathcal{L}_{\tilde{\chi}^+\tilde{\chi}^+ Z} = \frac{g}{c_W} Z_\mu \bar{\tilde{\chi}}_i^+ \gamma^\mu (O'^L_{ij} P_L + O'^R_{ij} P_R) \tilde{\chi}_j^+ - eA_\mu \bar{\tilde{\chi}}_i^+ \gamma^\mu \tilde{\chi}_i^+ \qquad \text{(A4)}$$

with $i, j = 1, 2$, and

$$O'^L_{ij} = -V_{i1}V^*_{j1} - \tfrac{1}{2}V_{i2}V^*_{j2} + \delta_{ij}\sin^2\theta_W, \qquad \text{(A5)}$$

$$O'^R_{ij} = -U^*_{i1}U_{j1} - \tfrac{1}{2}U^*_{i2}U_{j2} + \delta_{ij}\sin^2\theta_W. \qquad \text{(A6)}$$

3. Neutralino-chargino-W

The neutralino-chargino-W interaction is described by ($i = 1, 2$; $j = 1, \ldots, 4$)

$$\mathcal{L}_{\tilde{\chi}\tilde{\chi}W} = gW_\mu^- \bar{\tilde{\chi}}_j^0 \gamma^\mu (O_{ji}^L P_L + O_{ji}^R P_R)\tilde{\chi}_i^+ + gW_\mu^+ \bar{\tilde{\chi}}_i^+ \gamma^\mu (O_{ji}^{L*} P_L + O_{ji}^{R*} P_R)\tilde{\chi}_j^0 \quad \text{(A7)}$$

with

$$O_{ji}^L = N_{j2}V_{i1}^* - \frac{1}{\sqrt{2}}N_{j4}V_{i2}^* \quad \text{and} \quad O_{ji}^R = N_{j2}^* U_{i1} + \frac{1}{\sqrt{2}}N_{j3}^* U_{i2}. \quad \text{(A8)}$$

4. Neutralino-fermion-sfermion

The sfermion interaction with neutralinos is ($i = 1, 2$; $j = 1, \ldots, 4$)

$$\begin{aligned}\mathcal{L}_{f\tilde{f}\tilde{\chi}^0} &= g\bar{f}(f_{Lj}^{\tilde{f}} P_R + h_{Lj}^{\tilde{f}} P_L)\tilde{\chi}_j^0 \tilde{f}_L + g\bar{f}(h_{Rj}^{\tilde{f}} P_R \\ &\quad + f_{Rj}^{\tilde{f}} P_L)\tilde{\chi}_j^0 \tilde{f}_R + \text{H.c.} \\ &= g\bar{f}(a_{ij}^{\tilde{f}} P_R + b_{ij}^{\tilde{f}} P_L)\tilde{\chi}_j^0 \tilde{f}_i + \text{H.c.} \end{aligned} \quad \text{(A9)}$$

where

$$a_{ij}^{\tilde{f}} = f_{Lj}^{\tilde{f}} R_{1i}^{\tilde{f}} + h_{Rj}^{\tilde{f}} R_{2i}^{\tilde{f}}, \quad \text{(A10)}$$

$$b_{ij}^{\tilde{f}} = h_{Lj}^{\tilde{f}} R_{1i}^{\tilde{f}} + f_{Rj}^{\tilde{f}} R_{2i}^{\tilde{f}}. \quad \text{(A11)}$$

The couplings $f_{L,R}^{\tilde{f}}$ and $h_{L,R}^{\tilde{f}}$ are

$$f_{Lj}^{\tilde{t}} = -\frac{1}{\sqrt{2}}\left(N_{j2} + \frac{1}{3}\tan\theta_W N_{j1}\right), \quad f_{Lj}^{\tilde{b}} = \frac{1}{\sqrt{2}}\left(N_{j2} - \frac{1}{3}\tan\theta_W N_{j1}\right), \quad \text{(A12)}$$

$$f_{Rj}^{\tilde{t}} = \frac{2\sqrt{2}}{3}\tan\theta_W N_{j1}^*, \qquad f_{Rj}^{\tilde{b}} = -\frac{\sqrt{2}}{3}\tan\theta_W N_{j1}^*, \quad \text{(A13)}$$

$$h_{Rj}^{\tilde{t}} = -h_t^* N_{j4} = h_{Lj}^{\tilde{t}*}, \qquad h_{Rj}^{\tilde{b}} = -h_b^* N_{j3} = h_{Lj}^{\tilde{b}*} \quad \text{(A14)}$$

for stops and sbottoms, and

$$f_{Lj}^{\tilde{\tau}} = \frac{1}{\sqrt{2}}(\tan\theta_W N_{j1} + N_{j2}), \quad \text{(A15)}$$

$$f_{Rj}^{\tilde{\tau}} = -\sqrt{2}\tan\theta_W N_{j1}^*, \quad \text{(A16)}$$

$$h_{Rj}^{\tilde{\tau}} = -h_\tau^* N_{j3} = h_{Lj}^{\tilde{\tau}*} \quad \text{(A17)}$$

for staus. In more general terms,

$$f_{Lj}^{\tilde{f}} = -\sqrt{2}((e_f - I_{3L}^f)\tan\theta_W N_{j1} + I_{3L}^f N_{j2}), \quad f_{Rj}^{\tilde{f}} = \sqrt{2}e_f \tan\theta_W N_{j1}^*. \quad \text{(A18)}$$

5. Chargino-fermion-sfermion

The sfermion interaction with charginos is ($i, j = 1, 2$)

$$\begin{aligned}\mathcal{L}_{f'\tilde{f}\tilde{\chi}^\pm} &= g\bar{u}(-U_{j1}P_R + h_u V_{j2}^* P_L)\tilde{\chi}_j^+ \tilde{d}_L \\ &\quad + g\bar{u}(h_d^* U_{j2} P_R)\tilde{\chi}_j^+ \tilde{d}_R + g\bar{d}(-V_{j1}P_R \\ &\quad + h_d U_{j2}^* P_L)\tilde{\chi}_j^{+c}\tilde{u}_L + g\bar{d}(h_u^* V_{j2} P_R)\tilde{\chi}_j^{+c}\tilde{u}_R + \text{H.c.} \\ &= g\bar{u}(l_{ij}^{\tilde{d}} P_R + k_{ij}^{\tilde{d}} P_L)\tilde{\chi}_j^+ \tilde{d}_i \\ &\quad + g\bar{d}(l_{ij}^{\tilde{u}} P_R + k_{ij}^{\tilde{u}} P_L)\tilde{\chi}_j^{+c}\tilde{u}_i + \text{H.c.} \end{aligned} \quad \text{(A19)}$$

where u ($\tilde{u}$) stands for up-type (s)quarks and (s)neutrinos, and d ($\tilde{d}$) stands for down-type (s)quarks and charged (s)leptons. The couplings l and k are

$$l_{ij}^{\tilde{t}} = -V_{j1}R_{1i}^{\tilde{t}} + h_t^* V_{j2} R_{2i}^{\tilde{t}}, \quad l_{ij}^{\tilde{b}} = -U_{j1}R_{1i}^{\tilde{b}} + h_b^* U_{j2} R_{2i}^{\tilde{b}}, \quad \text{(A20)}$$

$$k_{ij}^{\tilde{t}} = h_b U_{j2}^* R_{1i}^{\tilde{t}}, \qquad k_{ij}^{\tilde{b}} = h_t V_{j2}^* R_{1i}^{\tilde{b}}, \quad \text{(A21)}$$

for stops and sbottoms, and

$$l_j^{\tilde{\nu}} = -V_{j1}, \qquad l_{ij}^{\tilde{\tau}} = -U_{j1}R_{1i}^{\tilde{\tau}} + h_\tau^* U_{j2} R_{2i}^{\tilde{\tau}}, \quad \text{(A22)}$$

$$k_j^{\tilde{\nu}} = h_\tau U_{j2}^*, \qquad k_{ij}^{\tilde{\tau}} = 0 \quad \text{(A23)}$$

for staus and sneutrinos.

6. Sfermions with gauge bosons

The sfermion interaction with photons is the same as in the *CP*-conserving case:

$$\begin{aligned}\mathcal{L}_{\tilde{f}\tilde{f}\gamma} &= -iee_f A_\mu (\tilde{f}_L^* \overleftrightarrow{\partial^\mu} \tilde{f}_L + \tilde{f}_R^* \overleftrightarrow{\partial^\mu} \tilde{f}_R) \\ &= -iee_f \delta_{ij} A_\mu \tilde{f}_j^* \overleftrightarrow{\partial^\mu} \tilde{f}_i. \end{aligned} \quad \text{(A24)}$$

The interaction with Z bosons is given by

$$\begin{aligned}\mathcal{L}_{\tilde{f}\tilde{f}Z} &= -\frac{ig}{\cos\theta_W} Z_\mu (C_L \tilde{f}_L^* \overleftrightarrow{\partial^\mu} \tilde{f}_L + C_R \tilde{f}_R^* \overleftrightarrow{\partial^\mu} \tilde{f}_R) \\ &= -\frac{ig}{\cos\theta_W}(C_L R_{1i}^{\tilde{f}} R_{1j}^{\tilde{f}*} + C_R R_{2i}^{\tilde{f}} R_{2j}^{\tilde{f}*}) Z_\mu \tilde{f}_j^* \overleftrightarrow{\partial^\mu} \tilde{f}_i \end{aligned} \quad \text{(A25)}$$

with $C_{L,R} = I_{3L,R}^f - e_f \sin^2\theta_W$. Note that there is only a phase dependence for $i \neq j$. The interaction with W bosons is given by

$$\mathcal{L}_{\tilde{f}\tilde{f}'W} = -\frac{ig}{\sqrt{2}}(W_\mu^+ \tilde{t}_L^* \overleftrightarrow{\partial^\mu} \tilde{b}_L + W_\mu^- \tilde{b}_R^* \overleftrightarrow{\partial^\mu} \tilde{t}_R)$$
$$= -\frac{ig}{\sqrt{2}}(R_{1i}^{\tilde{b}} R_{1j}^{\tilde{t}*} W_\mu^+ \tilde{t}_j^* \overleftrightarrow{\partial^\mu} \tilde{b}_i + R_{1i}^{\tilde{t}} R_{1j}^{\tilde{b}*} W_\mu^- \tilde{b}_j^* \overleftrightarrow{\partial^\mu} \tilde{t}_i) \tag{A26}$$

taking $\tilde{t}\,\tilde{b}\,W$ as an example for simplicity. The corresponding Feynman rules are obtained from

$$A\overleftrightarrow{\partial^\mu}B = A(\partial_\mu B) - (\partial_\mu A)B \rightarrow \tilde{f}_j^* \overleftrightarrow{\partial^\mu} \tilde{f}_i = i(k_i + k_j)^\mu \tag{A27}$$

where k_i and k_j are the four-momenta of $\tilde{f}_i$ and $\tilde{f}_j$ in the direction of the charge flow.

[1] G. Bertone, D. Hooper, and J. Silk, Phys. Rep. **405**, 279 (2005).
[2] C. L. Bennett *et al.*, Astrophys. J. Suppl. Ser. **148**, 1 (2003).
[3] D. N. Spergel *et al.* (WMAP Collaboration), Astrophys. J. Suppl. Ser. **148**, 175 (2003).
[4] M. Tegmark *et al.* (SDSS Collaboration), Phys. Rev. D **69**, 103501 (2004).
[5] H. Goldberg, Phys. Rev. Lett. **50**, 1419 (1983).
[6] J. R. Ellis, J. S. Hagelin, D. V. Nanopoulos, K. A. Olive, and M. Srednicki, Nucl. Phys. **B238**, 453 (1984).
[7] E. W. Kolb and M. S. Turner, *The Early Universe* (Addison-Wesley, New York, 1990).
[8] G. Belanger, F. Boudjema, A. Pukhov, and A. Semenov, Comput. Phys. Commun. **174**, 577 (2006).
[9] G. Belanger, F. Boudjema, A. Pukhov, and A. Semenov, Comput. Phys. Commun. **149**, 103 (2002).
[10] P. Gondolo *et al.*, J. Cosmol. Astropart. Phys. 07 (2004) 008.
[11] H. Baer, C. Balazs, and A. Belyaev, J. High Energy Phys. 03 (2002) 042.
[12] S. Profumo and C. E. Yaguna, Phys. Rev. D **70**, 095004 (2004).
[13] B. C. Allanach, G. Belanger, F. Boudjema, and A. Pukhov, J. High Energy Phys. 12 (2004) 020.
[14] N. Arkani-Hamed, A. Delgado, and G. F. Giudice, Nucl. Phys. **B741**, 108 (2006).
[15] M. Drees and M. M. Nojiri, Phys. Rev. D **47**, 376 (1993).
[16] L. Roszkowski, R. Ruiz de Austri, and T. Nihei, J. High Energy Phys. 08 (2001) 024.
[17] J. R. Ellis, K. A. Olive, Y. Santoso, and V. C. Spanos, Phys. Lett. B **565**, 176 (2003).
[18] C. Pallis and M. E. Gomez, hep-ph/0303098.
[19] H. Baer and C. Balazs, J. Cosmol. Astropart. Phys. 05 (2003) 006.
[20] A. B. Lahanas and D. V. Nanopoulos, Phys. Lett. B **568**, 55 (2003).
[21] U. Chattopadhyay, A. Corsetti, and P. Nath, Phys. Rev. D **68**, 035005 (2003).
[22] E. A. Baltz and P. Gondolo, J. High Energy Phys. 10 (2004) 052.
[23] G. Belanger, S. Kraml, and A. Pukhov, Phys. Rev. D **72**, 015003 (2005).
[24] B. C. Allanach and C. G. Lester, Phys. Rev. D **73**, 015013 (2006).
[25] A. Djouadi, M. Drees, and J.-L. Kneur, J. High Energy Phys. 03 (2006) 033.
[26] R. Arnowitt, B. Dutta, and Y. Santoso, Nucl. Phys. **B606**, 59 (2001).
[27] J. R. Ellis, T. Falk, K. A. Olive, and Y. Santoso, Nucl. Phys. **B652**, 259 (2003).
[28] A. Birkedal-Hansen and B. D. Nelson, Phys. Rev. D **67**, 095006 (2003).
[29] V. Bertin, E. Nezri, and J. Orloff, J. High Energy Phys. 02 (2003) 046.
[30] P. Binetruy, Y. Mambrini, and E. Nezri, Astropart. Phys. **22**, 1 (2004).
[31] H. Baer, A. Mustafayev, S. Profumo, A. Belyaev, and X. Tata, Phys. Rev. D **71**, 095008 (2005).
[32] G. Belanger, F. Boudjema, A. Cottrant, A. Pukhov, and A. Semenov, Nucl. Phys. **B706**, 411 (2005).
[33] H. Baer, A. Mustafayev, S. Profumo, A. Belyaev, and X. Tata, J. High Energy Phys. 07 (2005) 065.
[34] S. F. King and J. P. Roberts, hep-ph/0603095.
[35] R. Barate *et al.* (LEP Working Group), Phys. Lett. B **565**, 61 (2003).
[36] C. Balazs, M. Carena, A. Menon, D. E. Morrissey, and C. E. M. Wagner, Phys. Rev. D **71**, 075002 (2005).
[37] T. Konstandin, T. Prokopec, M. G. Schmidt, and M. Seco, Nucl. Phys. **B738**, 1 (2006), and references therein.
[38] V. Cirigliano, S. Profumo, and M. J. Ramsey-Musolf, hep-ph/0603246.
[39] D. Delepine, J. M. Gerard, R. Gonzalez Felipe, and J. Weyers, Phys. Lett. B **386**, 183 (1996).
[40] C. Balazs, M. Carena, and C. E. M. Wagner, Phys. Rev. D **70**, 015007 (2004).
[41] J. M. Cline and G. D. Moore, Phys. Rev. Lett. **81**, 3315 (1998).
[42] M. Carena, M. Quiros, and C. E. M. Wagner, Nucl. Phys. **B524**, 3 (1998).
[43] A. Pilaftsis, Phys. Lett. B **435**, 88 (1998).
[44] D. A. Demir, Phys. Rev. D **60**, 055006 (1999).
[45] A. Pilaftsis and C. E. M. Wagner, Nucl. Phys. **B553**, 3 (1999).
[46] T. Falk, K. A. Olive, and M. Srednicki, Phys. Lett. B **354**, 99 (1995).
[47] T. Nihei and M. Sasagawa, Phys. Rev. D **70**, 055011 (2004); **70**, 079901(E) (2004).
[48] M. Argyrou, A. B. Lahanas, D. V. Nanopoulos, and V. C. Spanos, Phys. Rev. D **70**, 095008 (2004); **70**, 119902(E) (2004)
[49] M. E. Gomez, T. Ibrahim, P. Nath, and S. Skadhauge, Phys. Rev. D **72**, 095008 (2005).
[50] P. Gondolo and K. Freese, J. High Energy Phys. 07 (2002)

052.
[51] S. Y. Choi and Y. G. Kim, Phys. Lett. B **637**, 27 (2006).
[52] G. Belanger, F. Boudjema, A. Pukhov, and A. Semenov, in Les Houches at Tev Colliders 2005: Beyond the Standard Model Working Group, summary report, B. C. Allanach *et al.*, hep-ph/0602198.
[53] G. Belanger, F. Boudjema, S. Kraml, A. Pukhov, and A. Semenov, in Les Houches at Tev Colliders 2005: Beyond the Standard Model Working Group, summary report, B. C. Allanach *et al.*, hep-ph/0602198.
[54] J. S. Lee *et al.*, Comput. Phys. Commun. **156**, 283 (2004).
[55] K. Hagiwara *et al.* (Particle Data Group), Phys. Rev. D **66**, 010001 (2002).
[56] P. Skands *et al.*, J. High Energy Phys. 07 (2004) 036.
[57] S. Y. Choi, M. Drees, J. S. Lee, and J. Song, Eur. Phys. J. C **25**, 307 (2002).
[58] P. Gondolo and G. Gelmini, Nucl. Phys. **B360**, 145 (1991).
[59] P. Gondolo and J. Edsjo, Phys. Rev. D **56**, 1879 (1997).
[60] A. V. Semenov, hep-ph/0208011.
[61] A. Pukhov, hep-ph/0412191.
[62] T. Ibrahim and P. Nath, Phys. Rev. D **58**, 111301 (1998); **60**, 099902(E) (1999).
[63] S. Y. Choi, M. Drees, and B. Gaissmaier, Phys. Rev. D **70**, 014010 (2004).
[64] D. Chang, W.-Y. Keung, and A. Pilaftsis, Phys. Rev. Lett. **82**, 900 (1999); **83**, 3972(E) (1999).
[65] A. Pilaftsis, Phys. Lett. B **471**, 174 (1999).
[66] D. A. Demir, O. Lebedev, K. A. Olive, M. Pospelov, and A. Ritz, Nucl. Phys. **B680**, 339 (2004).
[67] G. Belanger, F. Boudjema, A. Cottrant, A. Pukhov, and A. Semenov, Czech. J. Phys. **55**, B205 (2005).
[68] A. Masiero, S. Profumo, and P. Ullio, Nucl. Phys. **B712**, 86 (2005).
[69] Joint LEP2 SUSY Working Group (ALEPH, DELPHI, L3, OPAL Experiments), http://lepsusy.web.cern.ch/lepsusy.
[70] T. Nihei, Phys. Rev. D **73**, 035005 (2006).
[71] P. Bechtle (LEP Collaboration), Proc. Sci., HEP2005 (2005) 325 [hep-ex/0602046].
[72] H. Baer, A. Mustafayev, E.-K. Park, S. Profumo, and X. Tata, hep-ph/0603197.
[73] M. M. Nojiri, G. Polesello, and D. R. Tovey, J. High Energy Phys. 03 (2006) 063.
[74] R. Arnowitt, B. Dutta, T. Kamon, N. Kolev, and D. Toback, hep-ph/0603128.
[75] E. A. Baltz, M. Battaglia, M. E. Peskin, and T. Wizansky, hep-ph/0602187.
[76] H.-U. Martyn, hep-ph/0408226.
[77] P. Bambade, M. Berggren, F. Richard, and Z. Zhang, hep-ph/0406010.
[78] M. Drees, M. M. Nojiri, D. P. Roy, and Y. Yamada, Phys. Rev. D **56**, 276 (1997); **64**, 039901(E) (2001).
[79] L. Bergstrom and P. Ullio, Nucl. Phys. **B504**, 27 (1997).
[80] F. Boudjema, A. Semenov, and D. Temes, Phys. Rev. D **72**, 055024 (2005).
[81] D. N. Spergel *et al.*, astro-ph/0603449.